



CERN-EP-2024-229
06 September 2024

Multiplicity-dependent jet modification from di-hadron correlations in pp collisions at $\sqrt{s} = 13$ TeV

ALICE Collaboration*

Abstract

Short-range correlations between charged particles are studied via two-particle angular correlations in pp collisions at $\sqrt{s} = 13$ TeV. The correlation functions are measured as a function of the relative azimuthal angle $\Delta\phi$ and the pseudorapidity separation $\Delta\eta$ for pairs of primary charged particles within the pseudorapidity interval $|\eta| < 0.9$ and the transverse-momentum range $1 < p_T < 8$ GeV/c. Near-side ($|\Delta\phi| < 1.3$) peak widths are extracted from a generalised Gaussian fitted over the correlations in full pseudorapidity separation ($|\Delta\eta| < 1.8$), while the per-trigger associated near-side yields are extracted for the short-range correlations ($|\Delta\eta| < 1.3$). Both are evaluated as a function of charged-particle multiplicity obtained by two different event activity estimators. The width of the near-side peak decreases with increasing multiplicity, and this trend is reproduced qualitatively by the Monte Carlo event generators PYTHIA 8, AMPT, and EPOS. However, the models overestimate the width in the low transverse-momentum region ($p_T < 3$ GeV/c). The per-trigger associated near-side yield increases with increasing multiplicity. Although this trend is also captured qualitatively by the considered event generators, the yield is mostly overestimated by the models in the considered kinematic range. The measurement of the shape and yield of the short-range correlation peak can help us understand the interplay between jet fragmentation and event activity, quantify the narrowing trend of the near-side peak as a function of transverse momentum and multiplicity selections in pp collisions, and search for final-state jet modification in small collision systems.

arXiv:2409.04501v1 [nucl-ex] 6 Sep 2024

*See Appendix A for the list of collaboration members

1 Introduction

In high-energy particle collisions, measurements of particle correlations provide information on a wide range of physics effects, leading to quantitative and qualitative understanding of diverse phenomena in elementary (e.g. electron–positron), small (proton–proton and proton–nucleus), and large (nucleus–nucleus) collision systems. In fact, one of the first surprising results from the Large Hadron Collider (LHC) physics programme was the conclusive observation of correlations between particles across a wide range of pseudorapidity in pp collisions [1]. This was reminiscent of similar long-range correlations that had previously been observed in nucleus–nucleus (AA) collisions, and which had been attributed to the expansion of a hot and dense strongly-interacting medium produced in such interactions, the quark–gluon plasma (QGP) [2–6]. In heavy-ion collisions, measurements of correlations in momentum space give insight into both the collective *bulk* dynamics of the system expansion as well as the interactions of hard and soft probes with the surrounding medium [7]. Searches for similar signals in small collision systems is an active area of research. Current research in small collision systems focuses on varying system sizes to explore and identify the onset of signatures that are attributed to the formation of a QGP [8, 9].

In heavy-ion collisions, two- and multi-particle angular correlation measurements demonstrate that the produced medium exhibits strong *collectivity*, in which many particles show correlated behaviour despite being far apart in (pseudo)rapidity. The anisotropies in the azimuthal-angle distribution of the emitted final-state particles have been observed in nucleus–nucleus collisions from below 100A MeV up to Super Proton Synchrotron (SPS) energies (see Refs. [10–12] and references therein), in Au–Au collisions in the centre-of-mass energy range $4.5 < \sqrt{s_{NN}} < 200$ GeV at the Relativistic Heavy Ion Collider (RHIC) [2–5, 13, 14], and in Pb–Pb collisions at $\sqrt{s_{NN}} = 2.76$ and 5.02 TeV at the LHC [6, 15–17]. The anisotropy in the final-state momentum-space particle distribution is commonly explained as emerging from the initial-state spatial anisotropy through the pressure-driven expansion of strongly interacting matter, which in the SPS/RHIC/LHC energy regime is expected to be QGP. Models that describe the QGP expansion with hydrodynamic equations, such as SONIC [18] and MUSIC [19], are particularly successful in reproducing experimental measurements [20] of *anisotropic flow* [21]. While hydrodynamic models suggest that anisotropic flow arises predominantly from final-state interactions, other models posit an alternative description, in which the observed momentum anisotropy originates in the initial state. In particular, the interaction of dense colour fields in the colliding nuclei can produce a state known as the colour glass condensate in the early moments of the collision [22–24]. The resulting colour flux tubes may evolve to preferentially emit particles anisotropically in the azimuthal direction [25, 26]. To what extent these initial-state effects persist throughout the evolution of the collision, and give rise to final-state anisotropies consistent with experimental measurements, remains an open question.

In recent years, long-range correlations have been also observed in smaller collision systems such as proton–proton (pp) [27–32], proton–nucleus (pA) [33–36], and light nucleus–nucleus [37, 38] collisions. These results were surprising, as it was not expected that pp and pA collisions could produce the high energy density spread over a large spatial volume that is necessary for a medium to form. However, the origin of these long-range correlations in small systems is still not understood and is not clear whether they emerge due to the same underlying mechanisms as in the large collision systems.

Phenomenological Monte Carlo (MC) models based on Lund strings, such as PYTHIA [39, 40], are able to generate pp collisions with a large number of particles in the final state (high multiplicity) with colour reconnection, and anisotropy in the final-state momentum distributions by interactions of colour strings via a mechanism called *string shoving* [41]. However, they are not yet able to qualitatively describe the full range of QGP-like behaviour observed in small collision systems (see, for example, Ref. [42]). Alternative models based on rope fragmentation [43, 44] have also been developed.

Flow measurements in small collision systems present a significant experimental challenge due to the

contribution of non-flow correlations (processes that produce correlated particles which are not collective, namely jet fragmentation, as described below). In contrast to the case of heavy-ion collisions, in pp and pA collisions the relative amount of particles from the *bulk* (underlying event) is small, and therefore the characterisation of the jet fragmentation in small collision systems is necessary to accurately subtract non-flow effects and quantify potential biases in flow measurements.

In the hot and dense environment of a heavy-ion collision, the products of hard (high momentum transfer) parton-parton scatterings, known as *jets*, undergo strong interactions with the medium. The result is that the jet energy is redistributed to low-momentum particles, leading to a reduction in the number of high- p_T reconstructed jets and a modification of the momentum distribution of the jet fragments in AA collisions compared to pp collisions, a phenomenon known as *jet quenching* [45–47]. The first demonstration of this jet modification with two-particle correlations was observed in Au–Au collisions measured by the STAR experiment at RHIC [48]. Further studies of hadron–hadron and jet–hadron correlations at RHIC [49–54] and the LHC [55–61] have been used to quantitatively examine the jet structure in both pp and AA collisions to gain insight into the mechanisms of jet quenching in heavy-ion collisions (for a review, see Ref. [62]). Models which do not include a hot and dense medium like the QGP are currently unable to fully describe the jet suppression and momentum redistribution of jet fragments observed in nucleus–nucleus collisions [63, 64].

Anisotropic flow, which describes the bulk evolution of the medium, and jet quenching, which represents the interactions between the hard and soft components of the collision, are typically viewed as signatures of the strongly-interacting medium produced in heavy-ion collisions [65, 66]. However, while flow-like signals have been measured in small collision systems, the effects of jet quenching are expected to be small in pp and p–Pb collisions [67–73], and have not been observed within experimental uncertainties [74–83]. Experimental and theoretical efforts are essential to understand these two observations within the same underlying physics picture in collisions of small nuclei.

As an alternative approach to jet suppression measurements, in this work the angular distributions and per-trigger associated yields from jet fragmentation are studied as a function of charged-particle multiplicity in pp collisions at the centre-of-mass energy of $\sqrt{s} = 13$ TeV. Thus, this work is a complementary search for jet quenching effects in small collision systems, in which the modification of the jet fragmentation is quantified as a function of multiplicity and compared to MC models. Model comparisons are necessary to draw conclusions on whether the multiplicity-dependence of the jet fragmentation, examined via the yield of jet particles and the pseudorapidity width, are due to kinematic selections or presence of the QGP medium. Furthermore, this work provides input for studies of anisotropic flow by measuring the presence of non-flow as a function of relative pseudorapidity.

This article is organised into the following sections. First, the experimental setup and analysis method are described in Sec. 2 and Sec. 3, respectively. Section 4 discusses the systematic uncertainties. The results and their comparison with model calculations are presented and discussed in Sec. 5. Finally, the results are summarised in Sec. 6.

2 Experimental setup and data samples

The data sample of pp collisions at $\sqrt{s} = 13$ TeV used for the present analysis was recorded during the LHC Run 2 period from 2016 to 2018. A comprehensive description of the ALICE detector and its performance can be found in Refs. [6, 84, 85]. The analysis utilises the V0 detector [86], the Inner Tracking System (ITS) [87], and the Time Projection Chamber (TPC) [88].

The V0 detector consists of two arrays located on both sides of the interaction point, named V0A and V0C, each comprising 32 plastic scintillator tiles, covering the whole azimuthal angle within the pseudorapidity intervals $2.8 < \eta < 5.1$ and $-3.7 < \eta < -1.7$, respectively. The ITS is a silicon tracker

with six layers of silicon sensors. The two innermost layers of the ITS are called the Silicon Pixel Detector (SPD) [89]. The middle two layers are the Silicon Drift Detector, and the two outermost layers are the Silicon Strip Detector. The TPC is a gas-filled cylindrical tracking detector providing up to 159 reconstruction points for charged-particle tracks traversing the entire radial extent of the detector.

The V0 provides a minimum bias (MB) trigger in pp collisions. A time coincidence of V0A and V0C signals triggers the data collection. The amplitudes of V0A and V0C signals are proportional to charged-particle multiplicity and their sum is denoted as V0M. The V0M amplitude is utilised to define the multiplicity class. In addition to V0M, the multiplicity can be classified using the number of clusters in the outer layer of the SPD, which covers the acceptance $|\eta| < 1.4$ to measure the number of produced charged tracks at midrapidity, N_{ch} [27, 90]. The present paper utilises these two different multiplicity estimators covering different pseudorapidity ranges.

The analysed data samples of MB pp events at $\sqrt{s} = 13$ TeV correspond to an integrated luminosity (\mathcal{L}_{int}) of about 19 nb^{-1} [91]. The positions of primary vertices are reconstructed from track segments measured by the SPD. The reconstructed primary vertices are required to be within 8 cm of the nominal interaction point along the beam direction. Pileup events are identified as the events with multiple reconstructed primary vertices. These events are rejected if the longitudinal distance between any of the vertices to the main primary vertex is greater than 0.8 cm. The relative abundance of residual pileup events is estimated to range from 10^{-3} to 10^{-2} for MB events in pp collisions [92].

Charged-particle tracks are reconstructed in the pseudorapidity range $|\eta| < 0.9$ over the full azimuth with the TPC and the ITS detectors, which are located inside a large solenoidal magnet, providing a uniform magnetic field of 0.5 T oriented along the beam axis. To guarantee good track momentum resolution, the reconstructed tracks must have crossed at least 70 readout pad rows in the TPC and have at least two associated hits in the ITS, with at least one in the SPD. The distances of closest approach (DCA) of the track to the primary vertex in the longitudinal (d_z) and transverse (d_{xy}) directions are required to be $|d_z| < 2$ cm and $|d_{xy}| < (0.0105 + 0.0350 \times p_{\text{T}}^{-1.1})$ cm (with p_{T} in GeV/c), respectively, to suppress contamination from secondary charged particles originating from weakly decaying hadrons and interactions with the material. The contamination is strongest at low p_{T} and decreases from 9% for $p_{\text{T}} < 1$ GeV/c to less than 1% for $p_{\text{T}} > 10$ GeV/c [93]. The efficiency of charged-particle reconstruction is approximately 65% [94] at $p_{\text{T}} \sim 0.15$ GeV/c and increases to about 80% for particles with $p_{\text{T}} > 1$ GeV/c. The p_{T} resolution is approximately 1% for primary charged particles [95] with $p_{\text{T}} < 1$ GeV/c, and it linearly increases to 6% at $p_{\text{T}} \sim 50$ GeV/c in pp collisions [93]. In this article, *charged-particle* refers to a primary charged particle with a mean proper lifetime greater than 1 cm/c. This particle is either produced directly in the interaction or results from the decay of particles with a lifetime shorter than 1 cm/c, limited to decay chains leading to the interaction (see Ref. [95]).

3 Analysis procedure

The two-particle angular correlations are measured as a function of the relative azimuthal angle ($\Delta\phi$) and the relative pseudorapidity ($\Delta\eta$) of two charged particles, referred to as trigger and associated particles, and is divided by the number of trigger particles N_{trig} . The per-trigger yield is corrected for pair acceptance $B(\Delta\eta, \Delta\phi)$, which is calculated by associating trigger particles in a given event with particles from other events (event-mixing). The acceptance-corrected two-particle angular correlation can be expressed as

$$\frac{1}{N_{\text{trig}}} \frac{d^2 N_{\text{pair}}}{d\Delta\eta d\Delta\phi} = B(0, 0) \frac{S(\Delta\eta, \Delta\phi)}{B(\Delta\eta, \Delta\phi)} \Big|_{p_{\text{T, trig}}, p_{\text{T, assoc}}}, \quad (1)$$

where the number of trigger and associated particle pairs is denoted as N_{pair} . The transverse momenta of trigger and associated particles are denoted as $p_{\text{T, trig}}$ and $p_{\text{T, assoc}}$, where $p_{\text{T, trig}}$ is required to be higher than $p_{\text{T, assoc}}$. All tracks are within $|\eta| < 0.9$. The pair yield measured in the same event is represented

by $S(\Delta\eta, \Delta\phi)$. The longitudinal positions of the primary vertices of events to be mixed are required to be within the same, 2 cm wide, z_{vtx} interval for each multiplicity class used in this analysis.

The final correlation function is calculated by taking the weighted average of Eq. (1) results obtained in these individual bins [96, 97]. In addition, all primary tracks are corrected for the single-particle tracking efficiency in a given multiplicity class as a function of p_T , η , and z_{vtx} . The corrections for tracking efficiency and acceptance are constructed with MC simulations and are based on events generated with PYTHIA 8.3 with the Monash tune [40] and the GEANT3 transport package [98], which is employed to simulate the detector response.

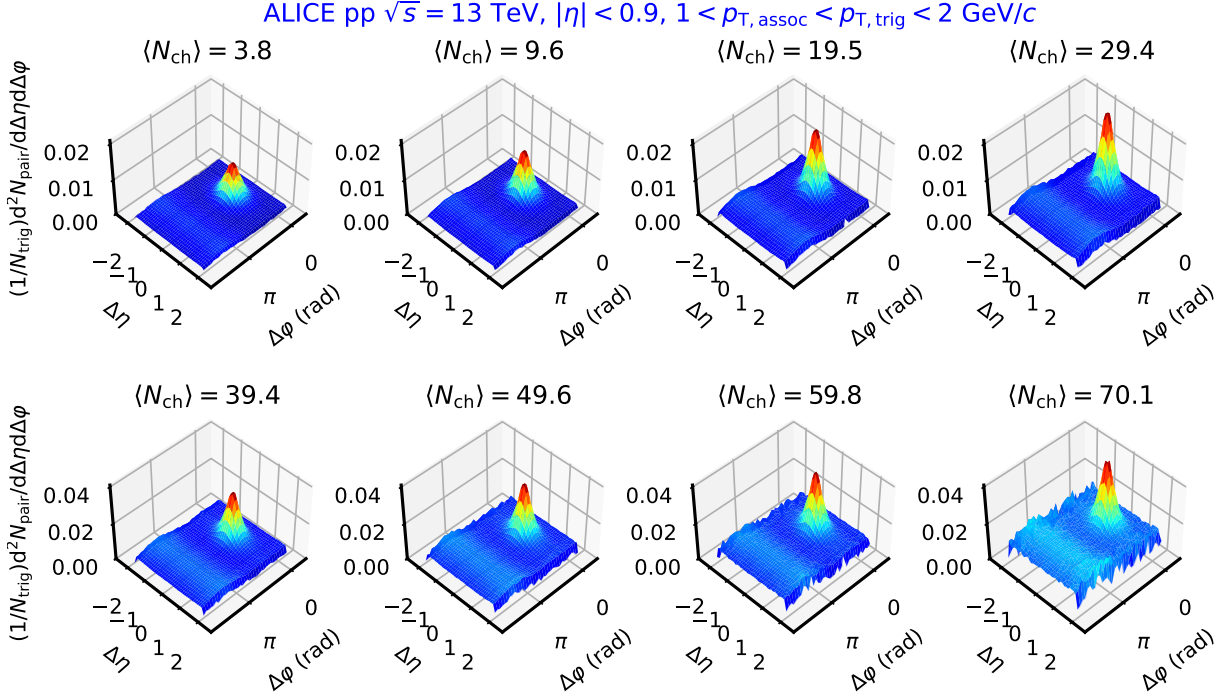


Figure 1: Two-particle angular correlation functions as a function of $\Delta\eta$ and $\Delta\phi$ in pp collisions at $\sqrt{s} = 13$ TeV for various multiplicity classes selected with the Midrapidity Multiplicity Estimator and characterised by the mean number of reconstructed tracks, $\langle N_{\text{ch}} \rangle$ ($|\eta| < 1.0$, $p_T > 0.2$ GeV/ c). All correlation functions are shown for $1 < p_{T, \text{assoc}} < p_{T, \text{trig}} < 2$ GeV/ c .

Figure 1 presents the fully corrected two-particle angular correlation functions in pp collisions at $\sqrt{s} = 13$ TeV for different multiplicity classes, which are classified with the mean number of reconstructed charged tracks at midrapidity ($\langle N_{\text{ch}} \rangle$), referred to as the *Midrapidity Multiplicity Estimator*. In order to correct for the effects of the tracking efficiency on the average multiplicity $\langle N_{\text{ch}} \rangle$, a correlation between the reconstructed and simulated multiplicities in the simulated samples is formed, which is then randomly sampled to obtain a new multiplicity value from the generated distribution corresponding to the reconstructed value [27, 90]. The prominent near-side jet fragmentation peak around $(\Delta\eta, \Delta\phi) \sim (0, 0)$ is mostly dominated by particle pairs coming from the same jet while the away-side region ($\Delta\phi \sim \pi$ and extended in the $\Delta\eta$ direction) is populated mostly by back-to-back jet correlations.

The shape of the jet fragmentation peak is quantified through a projection of the correlation function on to its $\Delta\eta$ -axis

$$\frac{1}{N_{\text{trig}}} \frac{dN_{\text{pair}}}{d\Delta\eta} = \int_{|\Delta\phi| < 1.3} \left(\frac{1}{N_{\text{trig}}} \frac{d^2N_{\text{pair}}}{d\Delta\eta d\Delta\phi} \right) \frac{1}{\delta_{\Delta\phi}} d\Delta\phi, \quad (2)$$

where $\delta_{\Delta\phi} = 2.6$ is the normalisation constant for the projection range, which is also used in the previous publication [97]. In order to characterise the near-side peak shape, the projected distribution is fitted with

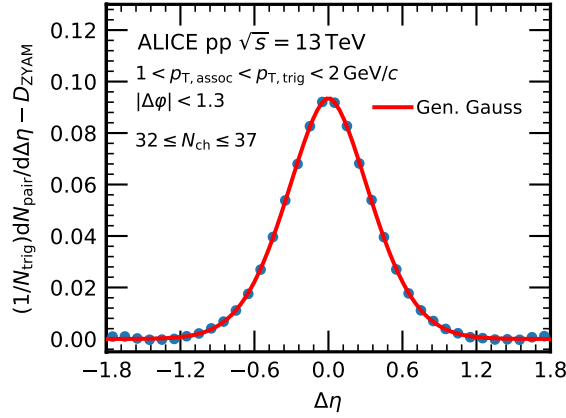


Figure 2: Near-side one-dimensional $\Delta\eta$ correlation function in pp collisions at $\sqrt{s} = 13$ TeV obtained using Eq. (2). The correlation is fitted with a generalised Gaussian distribution parameterised by Eq. (3). The projected correlation function is presented after the baseline subtraction (see text for details). The statistical uncertainties are smaller than the marker size, and the systematic uncertainties are not shown.

the generalised Gaussian function as shown in Fig. 2. This is pragmatic choice to characterise the shape without direct physics implications. The generalised Gaussian is given by

$$G_{\gamma_x, w_x}(x) = \frac{\gamma_x}{2w_x\Gamma(1/\gamma_x)} \exp\left[-\left(\frac{|x|}{w_x}\right)^{\gamma_x}\right] + A, \quad (3)$$

where w_x is the scale and γ_x the shape parameter. These parameters can be used to quantify the width of the near-side peak and provide information on the jet fragmentation pattern. Furthermore, Γ represents the Gamma function and A is a constant background pedestal. It is worth mentioning that $\gamma_x = 2$ and $\gamma_x = 1$ return Gaussian and Laplace distributions, respectively. The standard deviation (σ) of the generalised Gaussian function can be analytically expressed as $\sigma^2 \equiv w_x^2\Gamma(3/\gamma_x)/\Gamma(1/\gamma_x)$. Compared to the ordinary Gaussian, the generalised Gaussian function provides a better description of the projected correlation functions, especially in the region of large $\Delta\eta$ tails, which allows one to fit over the entire $\Delta\eta$ -range. Compared to the jet fragmentation peak, the small contribution of the near-side long-range correlations to the characterisation of its shape is considered negligible.

The near-side per-trigger associated yield ($Y_{\text{frag}}^{\text{near}}$) is measured by directly integrating the measured short-range $\Delta\eta$ correlations over $|\Delta\eta| < 1.3$ [27, 42], which can be expressed as

$$Y_{\text{frag}}^{\text{near}} = \int_{|\Delta\eta| < 1.3} \left(\frac{1}{N_{\text{trig}}} \frac{dN_{\text{pair}}}{d\Delta\eta} \right) d\Delta\eta - \delta_{\Delta\phi} D_{\text{ZYAM}}. \quad (4)$$

D_{ZYAM} defines the baseline of the ZYAM (Zero-Yield-at-Minimum) background subtraction [99], and is taken to be equal to the pedestal term of the fit, i.e. $D_{\text{ZYAM}} = A$, where A is from Eq. (3).

The same analysis procedure is used also for the other event-class definition used in this analysis based on the VOM amplitude, referred to as the *Forward Multiplicity Estimator*. The mean charged-particle multiplicity density ($\langle N_{\text{ch}} \rangle$) within $|\eta| < 1.0$ and $p_{\text{T}} > 0.2$ GeV/c for a given VOM percentile class is derived based on the corresponding $\langle N_{\text{ch}} \rangle$ for $|\eta| < 0.5$ and $p_{\text{T}} > 0$ GeV/c from Ref. [92]. This value is then scaled to match the kinematic ranges of the particles at midrapidity using PYTHIA 8 with the Monash tune [40]. This was repeated for all VOM amplitude percentiles. These values are corrected for acceptance and tracking efficiency, as well as for contamination by secondary particles.

4 Systematic uncertainties

The systematic uncertainties are evaluated by varying different selection criteria including the primary vertex position range, DCA selection range, track selection criteria, constraints on the particle charges, and efficiency correction, and looking for the deviations of the extracted observables with respect to the default setup. Unlike in the measurements of long-range correlations [27, 42], the $\Delta\eta$ and $\Delta\phi$ ranges are not varied, as these ranges are in the definition of the observable.

The sensitivity to detector acceptance effects is evaluated by varying the primary vertex position range for the event selection from $|z_{\text{vtx}}| < 8\text{ cm}$ to $|z_{\text{vtx}}| < 10\text{ cm}$. This effect is very small, of the order of 0–2% for the majority of the observables. The uncertainty emerging from the secondary track contributions is estimated by applying a tighter DCA selection in the beam direction, the DCA limits were changed from 2 cm to 0.3 cm. The resulting systematic uncertainty ranges from 0% to 2%. Different track selection criteria were tested. The uncertainty related to this choice, referred to as tracking mode, is obtained by changing track selection criteria to those used in Refs. [100, 101], which yield a more uniform azimuthal distribution of tracks. This uncertainty is found to be mostly between 1% to 3%. The possible impact of the contamination by resonance decays on the near-side peak width is tested by correlating two particles with the same charge (like-sign pair). The corresponding relative deviations of the observables between the default and like-sign pair analysis is below 3% at low p_{T} ($p_{\text{T}} < 1.5\text{ GeV}/c$) and increases up to 5–10% at high p_{T} ($p_{\text{T}} \sim 6\text{ GeV}/c$). Finally, the systematic uncertainty from the efficiency correction is evaluated from simulated data by comparing the results obtained with MC generated-level particles with those obtained with the corrected reconstruction-level particles. The resulting uncertainty is broadly around 5% for $p_{\text{T}} < 1.5\text{ GeV}/c$ and increases up to 10% at $p_{\text{T}} \sim 6\text{ GeV}/c$ or multiplicity $\langle N_{\text{ch}} \rangle \gtrsim 50$. The relative uncertainty resulting from the discrepancies in this closure test is the only source of uncertainty that differs significantly between the near-side jet width and yield observables, with the uncertainty on the width being typically much lower by 1–3% in all bins. The total systematic uncertainty is calculated by summing up each source in quadrature assuming no correlations between them. The total systematic uncertainty ranges between 3% and 15%, with mostly smaller values being achieved for lower p_{T} bins.

5 Results

Figure 3 presents the width of the near-side peak as a function of charged-particle multiplicity in pp collisions at $\sqrt{s} = 13\text{ TeV}$ for various $p_{\text{T, trig}}$ and $p_{\text{T, assoc}}$ intervals. The event activity is classified at midrapidity (left panel) and forward rapidity (right panel). For a given $p_{\text{T, trig}}$, the measured width decreases monotonously with increasing $p_{\text{T, assoc}}$ due to the boost of jet fragments. The decreasing trend is observed for both multiplicity estimators using charged particles at midrapidity and forward rapidity. The peak width also decreases as a function of $\langle N_{\text{ch}} \rangle$ for $p_{\text{T, assoc}} < 3\text{ GeV}/c$.

The narrowing trend of the near-side peak with increasing multiplicity is opposite to that observed in heavy-ion collisions for low $p_{\text{T, trig}}$ and $p_{\text{T, assoc}}$ intervals, where a broadening of the near-side peak is measured [58]. This happens only for the low associated- p_{T} intervals ($p_{\text{T}} < 2\text{ GeV}/c$), where the trend is strong. This trend as a function of multiplicity cannot be attributed solely to jet-quenching effects, which in heavy-ion collisions are considered to produce the broadening of the near-side peak. There may be a different kinematic bias from the multiplicity selection, which could obscure the clear identification of a possible jet-quenching signature in pp collisions. Additionally, other comprehensive studies, which have used jet reconstruction methods [79, 102], have independently reached similar conclusions.

Figure 4 shows the near-side peak yields as a function of charged-particle multiplicity at midrapidity in pp collisions at $\sqrt{s} = 13\text{ TeV}$ for various $p_{\text{T, trig}}$ and $p_{\text{T, assoc}}$ intervals and for the two event activity classifiers. The near-side yield increases with increasing multiplicity for both midrapidity and forward rapidity event multiplicity estimators. The trend increases more significantly as a function of the midrapidity than the forward rapidity multiplicity estimator due to auto-correlations [103].

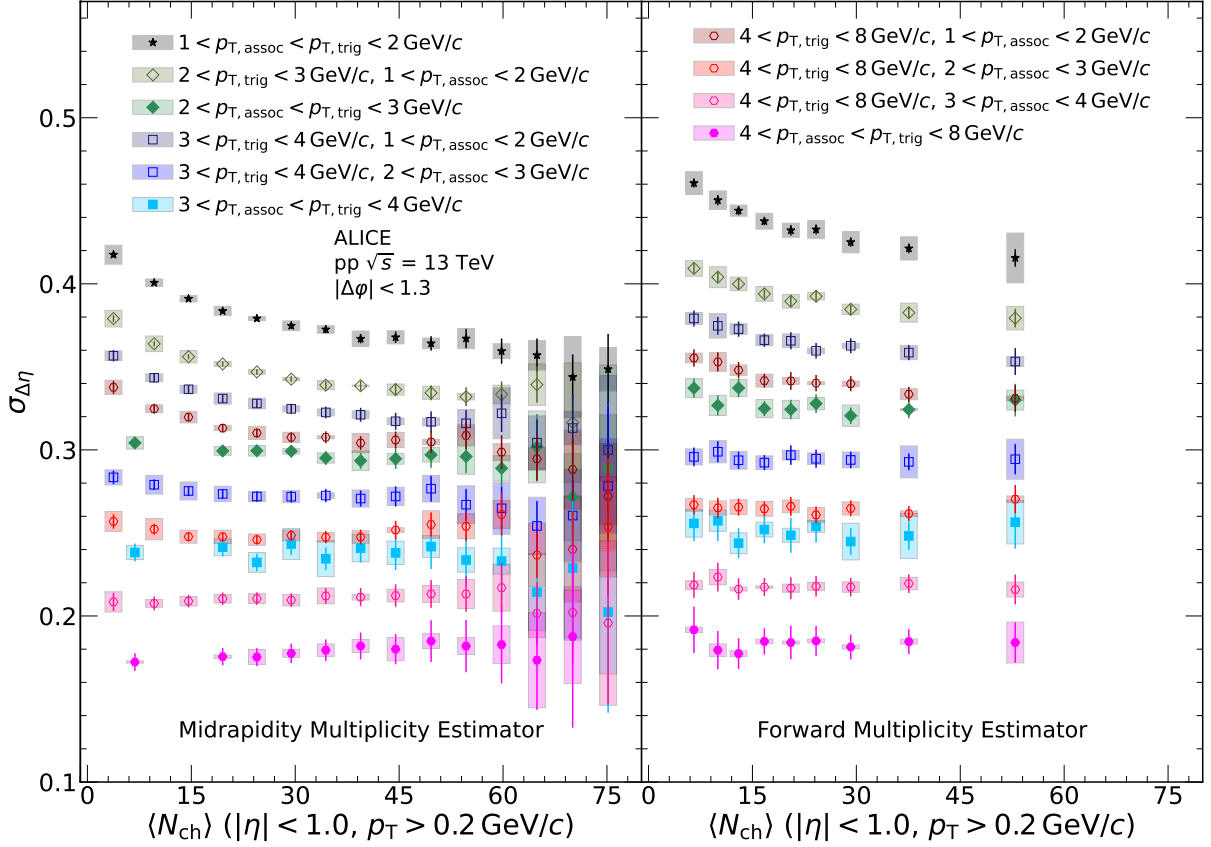


Figure 3: Near-side peak widths as a function of $\langle N_{\text{ch}} \rangle$ for all $p_{\text{T, trig}}$ and $p_{\text{T, assoc}}$ intervals. Results with event activity measured at midrapidity (forward rapidity) are shown on the left (right). The statistical and systematic uncertainties are displayed with error bars and boxes, respectively.

5.1 Comparisons with models

The measured data are compared with several MC event generators, namely PYTHIA 8, AMPT, and EPOS LHC. PYTHIA 8 [39] is a versatile event generator which can be used to simulate pp as well as heavy-ion collisions [63]. Some parameters of the PYTHIA 8 model, mostly the ones associated with the non-perturbative regime of quantum chromodynamics, are tuned to reproduce experimental data. The default parameter set of PYTHIA 8 is called the Monash tune. It was adjusted based on a large set of LHC measurements and can describe the production of soft particles relatively well [40]. Its predecessor, the tune 4C, which is tuned to the first LHC measurements [104], is used in this analysis for comparison to the more recent versions. In the default PYTHIA 8 versions, long-range correlations are not expected to emerge as there are no final-state partonic or hadronic interactions included. To describe these long-range correlations in HM pp collisions, string shoving can be enabled in PYTHIA 8 [41, 105]. This mechanism gives rise to a repulsive force acting between colour strings which yields a microscopic transverse pressure. The string shoving approach in PYTHIA 8 reproduces the experimental measurements by ALICE [42] and CMS [30] of the long-range near-side ($|\Delta\phi| < 1.3$) ridge yield in high-multiplicity (HM) pp events. One of the features of this model is that strings produced from hard scatterings are also affected by the repulsive force, which then leads to the observed long-range correlations even in low-multiplicity events with PYTHIA 8 [106].

The EPOS model uses a core–corona approach to describe the evolution of heavy-ion collisions [107]. The core is subject to hydrodynamic expansion, while the corona simulates the hadrons from string decays. Finally, UrQMD [108, 109] is used to model hadronic interactions of all hadrons coming from the corona or the hadronisation of the core. A version called EPOS LHC, which includes a different

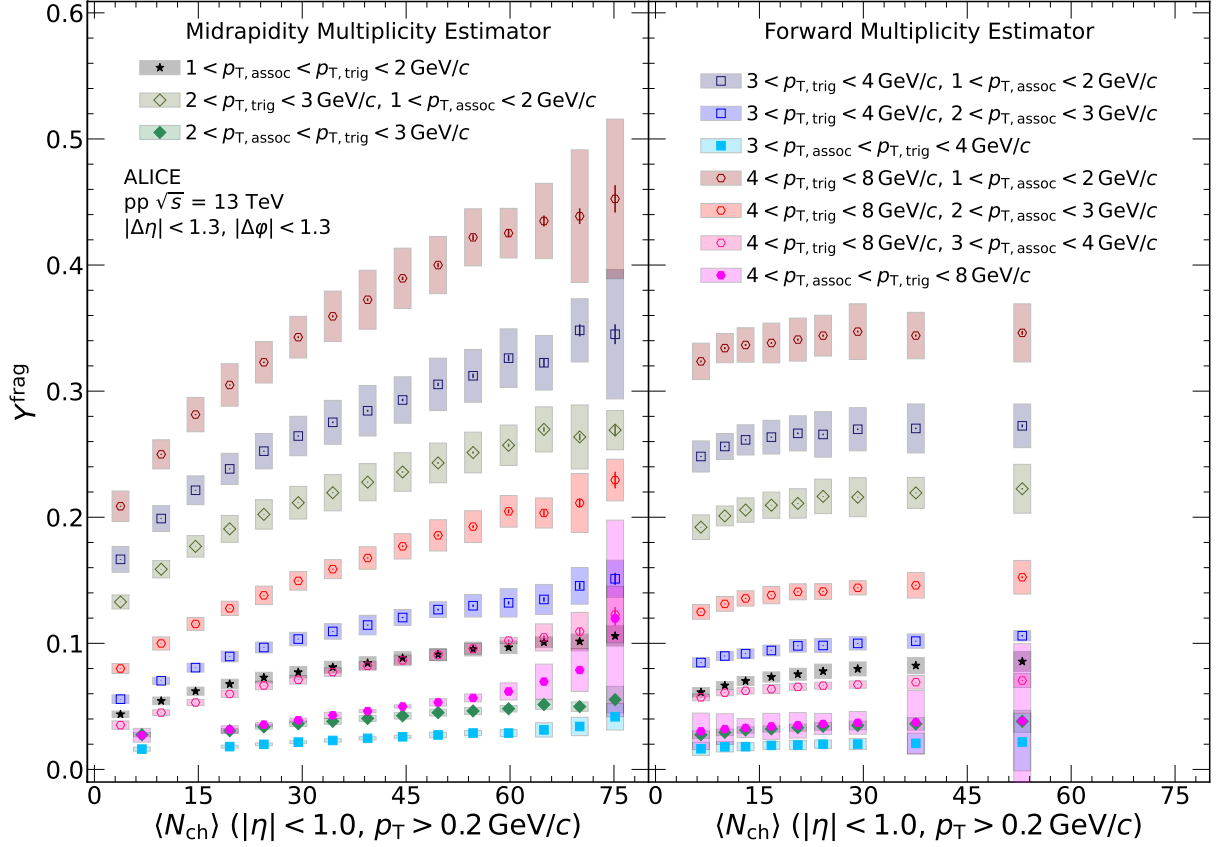


Figure 4: Per trigger normalised yield of associated particles in the near-side as a function of $\langle N_{ch} \rangle$ for all $p_{T, trig}$ and $p_{T, assoc}$ intervals. Results with event activity measured at midrapidity (forward rapidity) are shown on the left (right). The statistical and systematic uncertainties are displayed with error bars and boxes, respectively.

parameterisation of flow in the case of a small and dense system, can successfully describe the long-range correlations in HM pp events [42].

While models like EPOS [107] use a causal hydrodynamic framework in describing the collective phenomena in small collision systems, the AMPT model with string melting [110] does this by modelling the evolution of the medium as a collection of interacting partons and hadrons [111]. The applicability of the model in reproducing flow results in small systems is studied in Ref. [112]. The model can explain the long-range correlations for Pb–Pb collisions by introducing fluid-like and particle-like excitations with kinetic theory [113–115]. This study uses the same parton-interaction cross section value of 3 mb that is used in larger system studies [110]. This is important for the results to be comparable, as the partonic cross sections affect the final-state observables.

Figure 5 displays MC model comparisons with the measured near-side peak yields for the multiplicity classes selected with the midrapidity estimator. The models reproduce qualitatively the growth of the yields as a function of multiplicity. However, in lower p_T intervals for $\langle N_{ch} \rangle < 10$, the models predict a much steeper rise with increasing multiplicity. For the higher p_T intervals, the models agree better with the data. Similarly to the case of jet widths, the models overestimate the data for most p_T intervals with the exception of EPOS LHC, which underestimates the measured yields in all p_T intervals. Only in the highest p_T interval, the different PYTHIA 8 tunes can describe the data within uncertainties. The AMPT model (scaled by a factor of 0.6 in all panels for visibility) overestimates the yields in all p_T intervals, but captures the multiplicity dependence well in general.

Figure 6 compares the measured near-side peak widths with the MC model expectations for the multi-

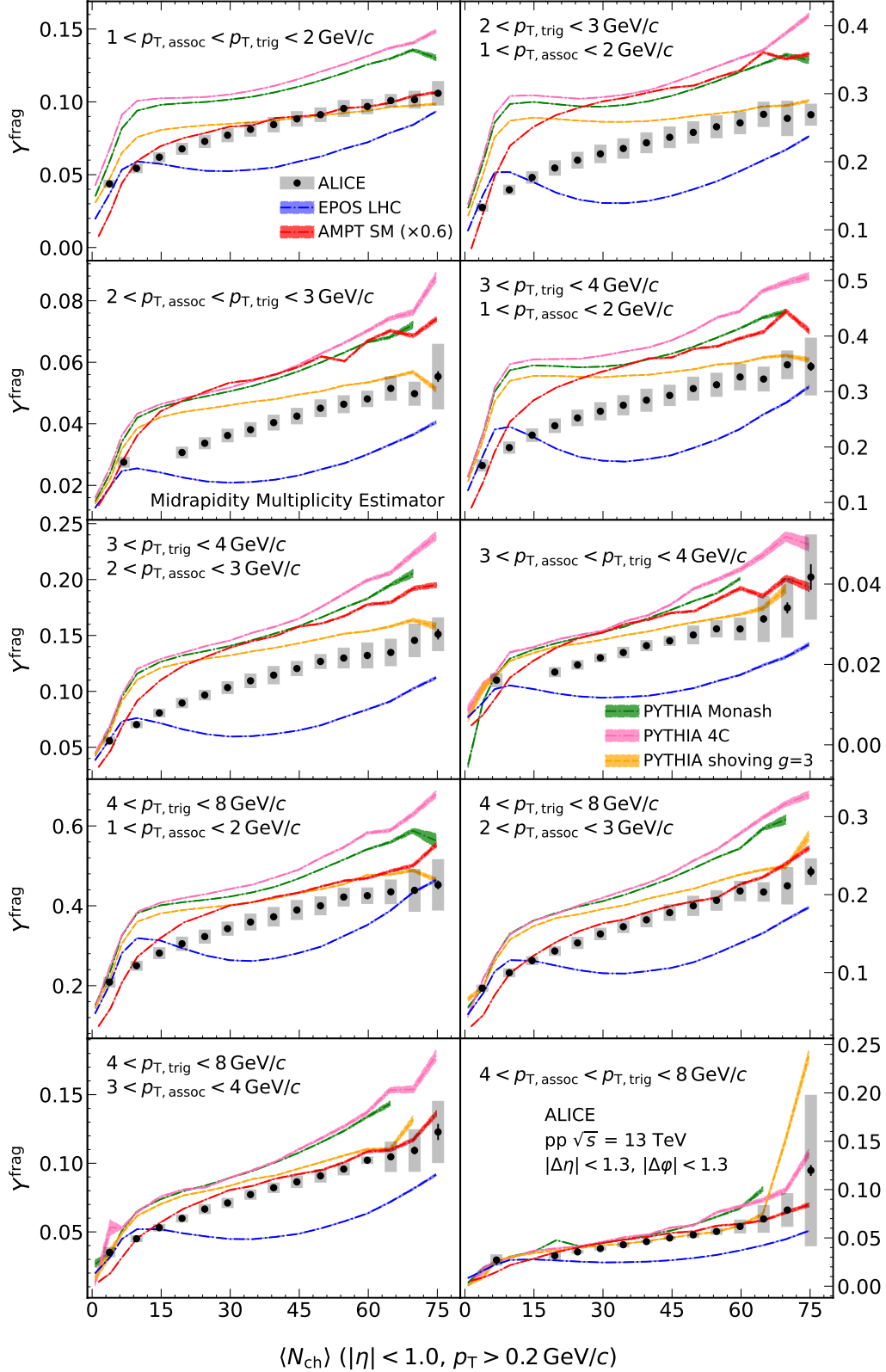


Figure 5: Multiplicity-dependence of near-side peak yields for all $p_{\text{T, trig}}$ and $p_{\text{T, assoc}}$ intervals measured in pp collisions at $\sqrt{s} = 13$ TeV, compared with MC models. Multiplicities are estimated at midrapidity. The model results are shown as coloured bands with the width of the band denoting the statistical uncertainties. The error bars (boxes) represent the statistical (systematic) uncertainties in the experimental data. The AMPT calculations are scaled by a factor of 0.6 in all panels for visibility.

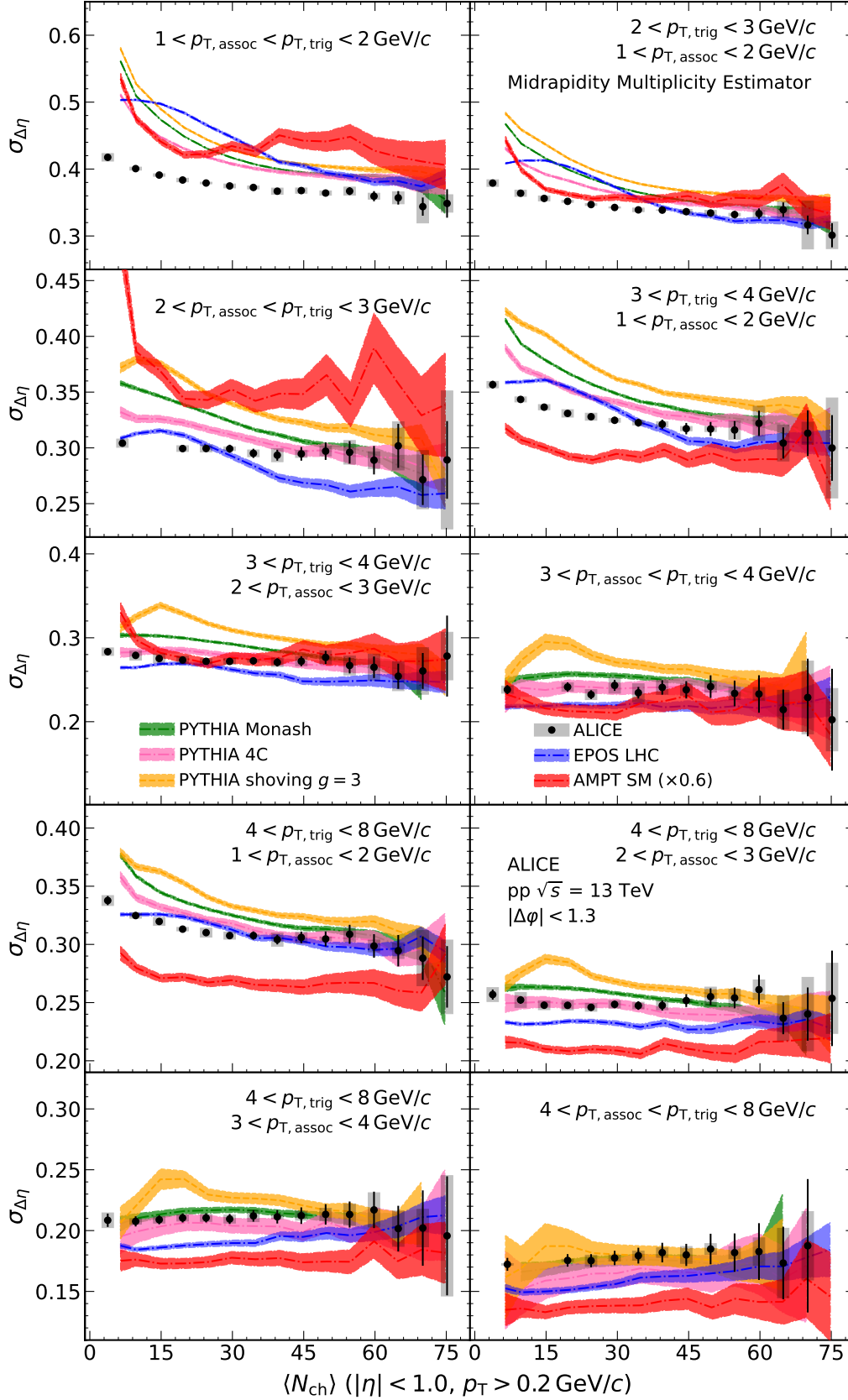


Figure 6: Multiplicity-dependence of near-side peak widths for all $p_{T, \text{trig}}$ and $p_{T, \text{assoc}}$ intervals measured in pp collisions at $\sqrt{s} = 13$ TeV, compared with MC models. Multiplicities are estimated at midrapidity. The model results are shown as coloured bands with the width of the band denoting the statistical uncertainties. The error bars (boxes) represent the statistical (systematic) uncertainties in the experimental data. The AMPT calculations are scaled by a factor of 0.6 in all panels for visibility.

plicity selection based on the midrapidity estimator. In all p_T intervals, except the two with $p_{T, \text{assoc}} > 3$ GeV/ c reported in the bottom panels of the figure, the simulated jet peaks get narrower with increasing multiplicity. The trend is stronger in the lower p_T intervals, while in the highest p_T intervals the multiplicity dependence becomes more flat. Interestingly, all models show similar multiplicity dependence with large overestimations of the near-side peak widths in the low multiplicity event classes. Furthermore, there is a subtle qualitative difference between the default PYTHIA 8 and PYTHIA 8 with string shoving, which suggests that the decreasing trend in the jet widths as a function of multiplicity might be connected to the final-state anisotropic particle distribution. In addition, the multiplicity dependence becomes weaker for the higher-multiplicity events, which is more prominent at lower p_T . All the models describe qualitatively the trend of the data, but overestimate the measured near-side peak widths in lower multiplicity classes and low p_T intervals. The largest discrepancy is observed for the AMPT model, which is for convenience scaled by a factor of 0.6 to fit in each of the panels. Yet, the AMPT model captures the multiplicity dependence of the near-side peak width. The PYTHIA 8 predictions and the data agree within uncertainties for $p_{T, \text{assoc}} > 3$ GeV/ c , where the trend is flat. Although, the model uncertainties are larger in the highest p_T interval, the best description of the data is provided by the 4C-tune. EPOS LHC presents a roughly similar magnitude and multiplicity dependence as the PYTHIA 8 models.

For all the considered PYTHIA 8 tunes, the predictions agree better with the data at higher p_T , specifically when $p_{T, \text{assoc}} > 3$ GeV/ c . PYTHIA 8 tends to provide a better description of the data in higher p_T intervals because in this region the perturbation theory becomes more relevant. This shows that improvement is needed in the non-perturbative (lower- p_T) regions. These results can be used as critical constraints for further model improvements, especially in studying differences in the equilibrium and non-equilibrium descriptions [116–122].

6 Conclusions

The multiplicity dependence of short-range correlations for pairs of charged particles is measured with the technique of two-particle angular correlations to search for jet-quenching effects in pp collisions at $\sqrt{s} = 13$ TeV. The shape and yield extracted from short-range correlations are measured as a function of the relative azimuthal angle $\Delta\phi$ and the pseudorapidity separation $\Delta\eta$ for pairs of primary charged particles within the pseudorapidity interval $|\eta| < 0.9$ and the transverse-momentum interval $1 < p_{T, \text{trig}} (\text{assoc}) < 8$ GeV/ c .

The near-side peak width and per-trigger associated yield, which are both related to jet fragmentation patterns, are extracted by fitting and integrating the short-range $\Delta\eta$ correlations within $|\Delta\eta| < 1.3$ and $|\Delta\phi| < 1.3$, in different multiplicity classes and p_T intervals. The near-side peak width monotonically decreases with increasing p_T due to the boost of evolving jet fragments. The near-side peak also gets narrower with increasing multiplicity for the low associated- p_T intervals ($p_T < 2$ GeV/ c). As discussed, the bias introduced by the measurement does not allow us to conclude on possible jet-fragmentation changes introduced by jet quenching. The jet fragmentation yield is significantly dependent on the transverse momenta of trigger and associated particles and are found to increase with increasing multiplicity.

The experimental data are compared with calculations from three event generators. All generators describe qualitatively the decreasing trend of the near-side jet peak width as a function of charged particle density, which manifests itself in lower p_T intervals, suggesting that the decreasing trend is attributed to kinematic selections rather than collective-like effects. Better descriptions are obtained from the models in higher p_T intervals, because there the system can be described more consistently with the perturbation theory. The narrowing trend of the near-side peak width toward HM events in experimental data and MC models suggests a potential bias in flow extraction methods that assume the independence of the near-side peak shape with multiplicity, such as the low-multiplicity (LM) template method [42]. Except for the EPOS LHC shown at the lowest p_T interval, the near-side yield is overestimated by the other

generators, although the considered PYTHIA 8 tunes describe the data better as p_T increases.

The measurement of the shape and yield of the near-side jet fragmentation peak is expected to provide a better understanding of particles emerging from jets and shows the narrowing trend of the peak width arising from kinematic selections in pp collisions. Such findings will help constrain models, provide information on biases in flow extraction methods, and contribute to the search for jet-quenching effects in small collision systems.

Acknowledgements

The ALICE Collaboration would like to thank all its engineers and technicians for their invaluable contributions to the construction of the experiment and the CERN accelerator teams for the outstanding performance of the LHC complex. The ALICE Collaboration gratefully acknowledges the resources and support provided by all Grid centres and the Worldwide LHC Computing Grid (WLCG) collaboration. The ALICE Collaboration acknowledges the following funding agencies for their support in building and running the ALICE detector: A. I. Alikhanyan National Science Laboratory (Yerevan Physics Institute) Foundation (ANSL), State Committee of Science and World Federation of Scientists (WFS), Armenia; Austrian Academy of Sciences, Austrian Science Fund (FWF): [M 2467-N36] and Nationalstiftung für Forschung, Technologie und Entwicklung, Austria; Ministry of Communications and High Technologies, National Nuclear Research Center, Azerbaijan; Conselho Nacional de Desenvolvimento Científico e Tecnológico (CNPq), Financiadora de Estudos e Projetos (Finep), Fundação de Amparo à Pesquisa do Estado de São Paulo (FAPESP) and Universidade Federal do Rio Grande do Sul (UFRGS), Brazil; Bulgarian Ministry of Education and Science, within the National Roadmap for Research Infrastructures 2020-2027 (object CERN), Bulgaria; Ministry of Education of China (MOEC), Ministry of Science & Technology of China (MSTC) and National Natural Science Foundation of China (NSFC), China; Ministry of Science and Education and Croatian Science Foundation, Croatia; Centro de Aplicaciones Tecnológicas y Desarrollo Nuclear (CEADEN), Cubaenergía, Cuba; Ministry of Education, Youth and Sports of the Czech Republic, Czech Republic; The Danish Council for Independent Research | Natural Sciences, the VILLUM FONDEN and Danish National Research Foundation (DNRF), Denmark; Helsinki Institute of Physics (HIP), Finland; Commissariat à l’Energie Atomique (CEA) and Institut National de Physique Nucléaire et de Physique des Particules (IN2P3) and Centre National de la Recherche Scientifique (CNRS), France; Bundesministerium für Bildung und Forschung (BMBF) and GSI Helmholtzzentrum für Schwerionenforschung GmbH, Germany; General Secretariat for Research and Technology, Ministry of Education, Research and Religions, Greece; National Research, Development and Innovation Office, Hungary; Department of Atomic Energy Government of India (DAE), Department of Science and Technology, Government of India (DST), University Grants Commission, Government of India (UGC) and Council of Scientific and Industrial Research (CSIR), India; National Research and Innovation Agency - BRIN, Indonesia; Istituto Nazionale di Fisica Nucleare (INFN), Italy; Japanese Ministry of Education, Culture, Sports, Science and Technology (MEXT) and Japan Society for the Promotion of Science (JSPS) KAKENHI, Japan; Consejo Nacional de Ciencia (CONACYT) y Tecnología, through Fondo de Cooperación Internacional en Ciencia y Tecnología (FONCICYT) and Dirección General de Asuntos del Personal Académico (DGAPA), Mexico; Nederlandse Organisatie voor Wetenschappelijk Onderzoek (NWO), Netherlands; The Research Council of Norway, Norway; Pontificia Universidad Católica del Perú, Peru; Ministry of Science and Higher Education, National Science Centre and WUT ID-UB, Poland; Korea Institute of Science and Technology Information and National Research Foundation of Korea (NRF), Republic of Korea; Ministry of Education and Scientific Research, Institute of Atomic Physics, Ministry of Research and Innovation and Institute of Atomic Physics and Universitatea Nationala de Stiinta si Tehnologie Politehnica Bucuresti, Romania; Ministry of Education, Science, Research and Sport of the Slovak Republic, Slovakia; National Research Foundation of South Africa, South Africa; Swedish Research Council (VR) and Knut & Alice Wallenberg Founda-

tion (KAW), Sweden; European Organization for Nuclear Research, Switzerland; Suranaree University of Technology (SUT), National Science and Technology Development Agency (NSTDA) and National Science, Research and Innovation Fund (NSRF via PMU-B B05F650021), Thailand; Turkish Energy, Nuclear and Mineral Research Agency (TENMAK), Turkey; National Academy of Sciences of Ukraine, Ukraine; Science and Technology Facilities Council (STFC), United Kingdom; National Science Foundation of the United States of America (NSF) and United States Department of Energy, Office of Nuclear Physics (DOE NP), United States of America. In addition, individual groups or members have received support from: Czech Science Foundation (grant no. 23-07499S), Czech Republic; FORTE project, reg. no. CZ.02.01.01/00/22_008/0004632, Czech Republic, co-funded by the European Union, Czech Republic; European Research Council (grant no. 950692), European Union; ICSC - Centro Nazionale di Ricerca in High Performance Computing, Big Data and Quantum Computing, European Union - NextGenerationEU; Academy of Finland (Center of Excellence in Quark Matter) (grant nos. 346327, 346328), Finland.

References

- [1] **CMS** Collaboration, V. Khachatryan *et al.*, “Observation of Long-Range Near-Side Angular Correlations in Proton-Proton Collisions at the LHC”, *JHEP* **09** (2010) 091, arXiv:1009.4122 [hep-ex].
- [2] **PHENIX** Collaboration, K. Adcox *et al.*, “Formation of dense partonic matter in relativistic nucleus-nucleus collisions at RHIC: Experimental evaluation by the PHENIX collaboration”, *Nucl. Phys.* **A757** (2005) 184–283, arXiv:nucl-ex/0410003 [nucl-ex].
- [3] **STAR** Collaboration, J. Adams *et al.*, “Experimental and theoretical challenges in the search for the quark gluon plasma: The STAR Collaboration’s critical assessment of the evidence from RHIC collisions”, *Nucl. Phys.* **A757** (2005) 102–183, arXiv:nucl-ex/0501009 [nucl-ex].
- [4] **BRAHMS** Collaboration, I. Arsene *et al.*, “Quark gluon plasma and color glass condensate at RHIC? The Perspective from the BRAHMS experiment”, *Nucl. Phys.* **A757** (2005) 1–27, arXiv:nucl-ex/0410020 [nucl-ex].
- [5] **PHOBOS** Collaboration, B. B. Back *et al.*, “The PHOBOS perspective on discoveries at RHIC”, *Nucl. Phys.* **A757** (2005) 28–101, arXiv:nucl-ex/0410022 [nucl-ex].
- [6] **ALICE** Collaboration, S. Acharya *et al.*, “The ALICE experiment: a journey through QCD”, *Eur. Phys. J. C* **84** (2024) 813, arXiv:2211.04384 [nucl-ex].
- [7] L. Apolinário, Y.-J. Lee, and M. Winn, “Heavy quarks and jets as probes of the QGP”, *Prog. Part. Nucl. Phys.* **127** (2022) 103990, arXiv:2203.16352 [hep-ph].
- [8] J. L. Nagle and W. A. Zajc, “Small System Collectivity in Relativistic Hadronic and Nuclear Collisions”, *Ann. Rev. Nucl. Part. Sci.* **68** (2018) 211–235, arXiv:1801.03477 [nucl-ex].
- [9] J. Brewer, A. Mazeliauskas, and W. van der Schee, “Opportunities of OO and pO collisions at the LHC”, in *Opportunities of OO and pO collisions at the LHC*. 3, 2021. arXiv:2103.01939 [hep-ph].
- [10] W. Reisdorf and H. G. Ritter, “Collective flow in heavy-ion collisions”, *Ann. Rev. Nucl. Part. Sci.* **47** (1997) 663–709.
- [11] N. Herrmann, J. P. Wessels, and T. Wienold, “Collective flow in heavy-ion collisions”, *Ann. Rev. Nucl. Part. Sci.* **49** (1999) 581–632.

- [12] S. A. Voloshin, A. M. Poskanzer, and R. Snellings, “Collective phenomena in non-central nuclear collisions”, *Landolt-Bornstein* **23** (2010) 293–333, arXiv:0809.2949 [nucl-ex].
- [13] **STAR** Collaboration, J. Adam *et al.*, “Flow and interferometry results from Au+Au collisions at $\sqrt{s_{NN}} = 4.5$ GeV”, *Phys. Rev. C* **103** (2021) 034908, arXiv:2007.14005 [nucl-ex].
- [14] **PHENIX** Collaboration, A. Adare *et al.*, “Dihadron azimuthal correlations in Au+Au collisions at $\sqrt{s_{NN}} = 200$ GeV”, *Phys. Rev. C* **78** (2008) 014901, arXiv:0801.4545 [nucl-ex].
- [15] **ALICE** Collaboration, B. Abelev *et al.*, “Anisotropic flow of charged hadrons, pions and (anti-)protons measured at high transverse momentum in Pb–Pb collisions at $\sqrt{s_{NN}} = 2.76$ TeV”, *Phys. Lett.* **B719** (2013) 18–28, arXiv:1205.5761 [nucl-ex].
- [16] **ALICE** Collaboration, B. Abelev *et al.*, “Elliptic flow of identified hadrons in Pb–Pb collisions at $\sqrt{s_{NN}} = 2.76$ TeV”, *JHEP* **06** (2015) 190, arXiv:1405.4632 [nucl-ex].
- [17] **ATLAS** Collaboration, G. Aad *et al.*, “Measurement of the pseudorapidity and transverse momentum dependence of the elliptic flow of charged particles in lead-lead collisions at $\sqrt{s_{NN}} = 2.76$ TeV with the ATLAS detector”, *Phys. Lett. B* **707** (2012) 330–348, arXiv:1108.6018 [hep-ex].
- [18] P. Romatschke, “Light-Heavy Ion Collisions: A window into pre-equilibrium QCD dynamics?”, *Eur. Phys. J. C* **75** (2015) 305, arXiv:1502.04745 [nucl-th].
- [19] B. Schenke, S. Jeon, and C. Gale, “(3+1)D hydrodynamic simulation of relativistic heavy-ion collisions”, *Phys. Rev. C* **82** (2010) 014903, arXiv:1004.1408 [hep-ph].
- [20] B. Schenke, S. Jeon, and C. Gale, “Elliptic and triangular flow in event-by-event (3+1)D viscous hydrodynamics”, *Phys. Rev. Lett.* **106** (2011) 042301, arXiv:1009.3244 [hep-ph].
- [21] J.-Y. Ollitrault, “Anisotropy as a signature of transverse collective flow”, *Phys. Rev. D* **46** (1992) 229–245.
- [22] L. D. McLerran and R. Venugopalan, “Gluon distribution functions for very large nuclei at small transverse momentum”, *Phys. Rev. D* **49** (1994) 3352–3355, arXiv:hep-ph/9311205.
- [23] L. D. McLerran and R. Venugopalan, “Computing quark and gluon distribution functions for very large nuclei”, *Phys. Rev. D* **49** (1994) 2233–2241, arXiv:hep-ph/9309289.
- [24] E. Iancu and R. Venugopalan, *The Color glass condensate and high-energy scattering in QCD*, pp. 249–3363. 3, 2003. arXiv:hep-ph/0303204.
- [25] A. Dumitru, K. Dusling, F. Gelis, J. Jalilian-Marian, T. Lappi, and R. Venugopalan, “The Ridge in proton-proton collisions at the LHC”, *Phys. Lett. B* **697** (2011) 21–25, arXiv:1009.5295 [hep-ph].
- [26] K. Dusling and R. Venugopalan, “Azimuthal collimation of long range rapidity correlations by strong color fields in high multiplicity hadron-hadron collisions”, *Phys. Rev. Lett.* **108** (2012) 262001, arXiv:1201.2658 [hep-ph].
- [27] **ALICE** Collaboration, S. Acharya *et al.*, “Emergence of Long-Range Angular Correlations in Low-Multiplicity Proton–Proton Collisions”, *Phys. Rev. Lett.* **132** (2024) 172302, arXiv:2311.14357 [nucl-ex].
- [28] **ATLAS** Collaboration, G. Aad *et al.*, “Observation of Long-Range Elliptic Azimuthal Anisotropies in $\sqrt{s} = 13$ and 2.76 TeV *pp* Collisions with the ATLAS Detector”, *Phys. Rev. Lett.* **116** (2016) 172301, arXiv:1509.04776 [hep-ex].

- [29] **CMS** Collaboration, V. Khachatryan *et al.*, “Measurement of long-range near-side two-particle angular correlations in pp collisions at $\sqrt{s} = 13$ TeV”, *Phys. Rev. Lett.* **116** (2016) 172302, arXiv:1510.03068 [nucl-ex].
- [30] **CMS** Collaboration, V. Khachatryan *et al.*, “Evidence for collectivity in pp collisions at the LHC”, *Phys. Lett. B* **765** (2017) 193–220, arXiv:1606.06198 [nucl-ex].
- [31] **ALICE** Collaboration, S. Acharya *et al.*, “Investigations of Anisotropic Flow Using Multiparticle Azimuthal Correlations in pp, p–Pb, Xe–Xe, and Pb–Pb Collisions at the LHC”, *Phys. Rev. Lett.* **123** (2019) 142301, arXiv:1903.01790 [nucl-ex].
- [32] **ATLAS** Collaboration, M. Aaboud *et al.*, “Measurement of long-range multiparticle azimuthal correlations with the subevent cumulant method in pp and p+Pb collisions with the ATLAS detector at the CERN Large Hadron Collider”, *Phys. Rev. C* **97** (2018) 024904, arXiv:1708.03559 [hep-ex].
- [33] **ALICE** Collaboration, B. Abelev *et al.*, “Long-range angular correlations on the near and away side in p–Pb collisions at $\sqrt{s_{NN}} = 5.02$ TeV”, *Phys. Lett. B* **719** (2013) 29–41, arXiv:1212.2001 [nucl-ex].
- [34] **ATLAS** Collaboration, G. Aad *et al.*, “Measurement of long-range pseudorapidity correlations and azimuthal harmonics in $\sqrt{s_{NN}} = 5.02$ TeV proton-lead collisions with the ATLAS detector”, *Phys. Rev. C* **90** (2014) 044906, arXiv:1409.1792 [hep-ex].
- [35] **ATLAS** Collaboration, M. Aaboud *et al.*, “Measurements of long-range azimuthal anisotropies and associated Fourier coefficients for pp collisions at $\sqrt{s} = 5.02$ and 13 TeV and p+Pb collisions at $\sqrt{s_{NN}} = 5.02$ TeV with the ATLAS detector”, *Phys. Rev. C* **96** (2017) 024908, arXiv:1609.06213 [nucl-ex].
- [36] **CMS** Collaboration, V. Khachatryan *et al.*, “Pseudorapidity dependence of long-range two-particle correlations in pPb collisions at $\sqrt{s_{NN}} = 5.02$ TeV”, *Phys. Rev. C* **96** (2017) 014915, arXiv:1604.05347 [nucl-ex].
- [37] **PHENIX** Collaboration, C. Aidala *et al.*, “Creation of quark–gluon plasma droplets with three distinct geometries”, *Nature Phys.* **15** (2019) 214–220, arXiv:1805.02973 [nucl-ex].
- [38] **PHENIX** Collaboration, C. Aidala *et al.*, “Measurements of Multiparticle Correlations in d + Au Collisions at 200, 62.4, 39, and 19.6 GeV and p + Au Collisions at 200 GeV and Implications for Collective Behavior”, *Phys. Rev. Lett.* **120** (2018) 062302, arXiv:1707.06108 [nucl-ex].
- [39] C. Bierlich *et al.*, “A comprehensive guide to the physics and usage of PYTHIA 8.3”, *SciPost Phys. Codeb.* **2022** (2022) 8, arXiv:2203.11601 [hep-ph].
- [40] P. Skands, S. Carrazza, and J. Rojo, “Tuning PYTHIA 8.1: the Monash 2013 Tune”, *Eur. Phys. J. C* **74** (2014) 3024, arXiv:1404.5630 [hep-ph].
- [41] C. Bierlich, G. Gustafson, and L. Lönnblad, “Collectivity without plasma in hadronic collisions”, *Phys. Lett. B* **779** (2018) 58–63, arXiv:1710.09725 [hep-ph].
- [42] **ALICE** Collaboration, S. Acharya *et al.*, “Long- and short-range correlations and their event-scale dependence in high-multiplicity pp collisions at $\sqrt{s} = 13$ TeV”, *JHEP* **05** (2021) 290, arXiv:2101.03110 [nucl-ex].
- [43] N. Fischer and T. Sjöstrand, “Thermodynamical String Fragmentation”, *JHEP* **01** (2017) 140, arXiv:1610.09818 [hep-ph].

- [44] A. Ortiz, G. Bencedi, and H. Bello, “Revealing the source of the radial flow patterns in proton–proton collisions using hard probes”, *J. Phys. G* **44** (2017) 065001, arXiv:1608.04784 [hep-ph].
- [45] M. Gyulassy, P. Levai, and I. Vitev, “Jet quenching in thin plasmas”, *Nucl. Phys. A* **661** (1999) 637–640, arXiv:hep-ph/9907343.
- [46] A. Majumder and M. Van Leeuwen, “The Theory and Phenomenology of Perturbative QCD Based Jet Quenching”, *Prog. Part. Nucl. Phys.* **66** (2011) 41–92, arXiv:1002.2206 [hep-ph].
- [47] L. Cunqueiro and A. M. Sickles, “Studying the QGP with Jets at the LHC and RHIC”, *Prog. Part. Nucl. Phys.* **124** (2022) 103940, arXiv:2110.14490 [nucl-ex].
- [48] **STAR** Collaboration, J. Adams *et al.*, “Evidence from d+Au measurements for final state suppression of high p_T hadrons in Au+Au collisions at RHIC”, *Phys. Rev. Lett.* **91** (2003) 072304, arXiv:nucl-ex/0306024.
- [49] **PHENIX** Collaboration, S. S. Adler *et al.*, “Dense-Medium Modifications to Jet-Induced Hadron Pair Distributions in Au+Au Collisions at $\sqrt{s_{NN}} = 200$ GeV”, *Phys. Rev. Lett.* **97** (2006) 052301, arXiv:nucl-ex/0507004.
- [50] **PHENIX** Collaboration, S. S. Adler *et al.*, “Jet properties from dihadron correlations in p+p collisions at $\sqrt{s} = 200$ GeV”, *Phys. Rev. D* **74** (2006) 072002, arXiv:hep-ex/0605039.
- [51] **PHENIX** Collaboration, A. Adare *et al.*, “Transverse momentum and centrality dependence of dihadron correlations in Au+Au collisions at $\sqrt{s_{NN}} = 200$ GeV: Jet-quenching and the response of partonic matter”, *Phys. Rev. C* **77** (2008) 011901, arXiv:0705.3238 [nucl-ex].
- [52] **STAR** Collaboration, M. M. Aggarwal *et al.*, “Azimuthal di-hadron correlations in d+Au and Au+Au collisions at $\sqrt{s_{NN}} = 200$ GeV from STAR”, *Phys. Rev. C* **82** (2010) 024912, arXiv:1004.2377 [nucl-ex].
- [53] **STAR** Collaboration, L. Adamczyk *et al.*, “Jet-Hadron Correlations in $\sqrt{s_{NN}} = 200$ GeV $p + p$ and Central Au + Au Collisions”, *Phys. Rev. Lett.* **112** (2014) 122301, arXiv:1302.6184 [nucl-ex].
- [54] **STAR** Collaboration, L. Adamczyk *et al.*, “Jet-like Correlations with Direct-Photon and Neutral-Pion Triggers at $\sqrt{s_{NN}} = 200$ GeV”, *Phys. Lett. B* **760** (2016) 689–696, arXiv:1604.01117 [nucl-ex].
- [55] **ALICE** Collaboration, K. Aamodt *et al.*, “Particle-yield modification in jet-like azimuthal di-hadron correlations in Pb–Pb collisions at $\sqrt{s_{NN}} = 2.76$ TeV”, *Phys. Rev. Lett.* **108** (2012) 092301, arXiv:1110.0121 [nucl-ex].
- [56] **CMS** Collaboration, V. Khachatryan *et al.*, “Correlations between jets and charged particles in PbPb and pp collisions at $\sqrt{s_{NN}} = 2.76$ TeV”, *JHEP* **02** (2016) 156, arXiv:1601.00079 [nucl-ex].
- [57] **CMS** Collaboration, V. Khachatryan *et al.*, “Measurement of transverse momentum relative to dijet systems in PbPb and pp collisions at $\sqrt{s_{NN}} = 2.76$ TeV”, *JHEP* **01** (2016) 006, arXiv:1509.09029 [nucl-ex].
- [58] **ALICE** Collaboration, J. Adam *et al.*, “Anomalous evolution of the near-side jet peak shape in Pb–Pb collisions at $\sqrt{s_{NN}} = 2.76$ TeV”, *Phys. Rev. Lett.* **119** (2017) 102301, arXiv:1609.06643 [nucl-ex].

- [59] **ALICE** Collaboration, J. Adam *et al.*, “Evolution of the longitudinal and azimuthal structure of the near-side jet peak in Pb–Pb collisions at $\sqrt{s_{\text{NN}}} = 2.76$ TeV”, *Phys. Rev. C* **96** (2017) 034904, arXiv:1609.06667 [nucl-ex].
- [60] **ALICE** Collaboration, J. Adam *et al.*, “Jet-like correlations with neutral pion triggers in pp and central Pb–Pb collisions at 2.76 TeV”, *Phys. Lett. B* **763** (2016) 238–250, arXiv:1608.07201 [nucl-ex].
- [61] **ALICE** Collaboration, S. Acharya *et al.*, “Jet fragmentation transverse momentum measurements from di-hadron correlations in $\sqrt{s} = 7$ TeV pp and $\sqrt{s_{\text{NN}}} = 5.02$ TeV p–Pb collisions”, *JHEP* **03** (2019) 169, arXiv:1811.09742 [nucl-ex].
- [62] M. Connors, C. Nattrass, R. Reed, and S. Salur, “Jet measurements in heavy ion physics”, *Rev. Mod. Phys.* **90** (2018) 025005, arXiv:1705.01974 [nucl-ex].
- [63] C. Bierlich, G. Gustafson, L. Lönnblad, and H. Shah, “The Angantyr model for Heavy-Ion Collisions in PYTHIA8”, *JHEP* **10** (2018) 134, arXiv:1806.10820 [hep-ph].
- [64] A. V. da Silva, W. M. Serenone, D. Dobrigkeit Chinellato, J. Takahashi, and C. Bierlich, “Studies of heavy-ion collisions using PYTHIA Angantyr and UrQMD”, arXiv:2002.10236 [hep-ph].
- [65] M. Gyulassy and M. Plumer, “Jet Quenching in Dense Matter”, *Phys. Lett. B* **243** (1990) 432–438.
- [66] X.-N. Wang and M. Gyulassy, “Gluon shadowing and jet quenching in $A + A$ collisions at $\sqrt{s_{\text{NN}}} = 200$ GeV”, *Phys. Rev. Lett.* **68** (1992) 1480–1483.
- [67] X. Zhang and J. Liao, “Jet Quenching and Its Azimuthal Anisotropy in AA and possibly High Multiplicity pA and dA Collisions”, arXiv:1311.5463 [nucl-th].
- [68] K. Tywoniuk, “Is there jet quenching in pPb?”, *Nucl. Phys. A* **926** (2014) 85–91.
- [69] C. Park, C. Shen, S. Jeon, and C. Gale, “Rapidity-dependent jet energy loss in small systems with finite-size effects and running coupling”, *Nucl. Part. Phys. Proc.* **289–290** (2017) 289–292, arXiv:1612.06754 [nucl-th].
- [70] A. Huss, A. Kurkela, A. Mazeliauskas, R. Paatelainen, W. van der Schee, and U. A. Wiedemann, “Predicting parton energy loss in small collision systems”, *Phys. Rev. C* **103** (2021) 054903, arXiv:2007.13758 [hep-ph].
- [71] A. Huss, A. Kurkela, A. Mazeliauskas, R. Paatelainen, W. van der Schee, and U. A. Wiedemann, “Discovering Partonic Rescattering in Light Nucleus Collisions”, *Phys. Rev. Lett.* **126** (2021) 192301, arXiv:2007.13754 [hep-ph].
- [72] B. G. Zakharov, “Jet quenching from heavy to light ion collisions”, *JHEP* **09** (2021) 087, arXiv:2105.09350 [hep-ph].
- [73] W. Ke and I. Vitev, “Searching for QGP droplets with high- p_{T} hadrons and heavy flavor”, *Phys. Rev. C* **107** (2023) 064903, arXiv:2204.00634 [hep-ph].
- [74] **ALICE** Collaboration, J. Adam *et al.*, “Centrality dependence of particle production in p–Pb collisions at $\sqrt{s_{\text{NN}}} = 5.02$ TeV”, *Phys. Rev. C* **91** (2015) 064905, arXiv:1412.6828 [nucl-ex].
- [75] **CMS** Collaboration, V. Khachatryan *et al.*, “Charged-particle nuclear modification factors in Pb–Pb and p–Pb collisions at $\sqrt{s_{\text{NN}}} = 5.02$ TeV”, *JHEP* **04** (2017) 039, arXiv:1611.01664 [nucl-ex].

- [76] **ALICE** Collaboration, J. Adam *et al.*, “Centrality dependence of charged jet production in p–Pb collisions at $\sqrt{s_{\text{NN}}} = 5.02$ TeV”, *Eur. Phys. J. C* **76** (2016) 271, arXiv:1603.03402 [nucl-ex].
- [77] **ALICE** Collaboration, J. Adam *et al.*, “Multiplicity dependence of charged pion, kaon, and (anti)proton production at large transverse momentum in p–Pb collisions at $\sqrt{s_{\text{NN}}} = 5.02$ TeV”, *Phys. Lett. B* **760** (2016) 720–735, arXiv:1601.03658 [nucl-ex].
- [78] **ALICE** Collaboration, S. Acharya *et al.*, “Constraints on jet quenching in p–Pb collisions at $\sqrt{s_{\text{NN}}} = 5.02$ TeV measured by the event-activity dependence of semi-inclusive hadron-jet distributions”, *Phys. Lett. B* **783** (2018) 95–113, arXiv:1712.05603 [nucl-ex].
- [79] **ALICE** Collaboration, S. Acharya *et al.*, “Search for jet quenching effects in high-multiplicity pp collisions at $\sqrt{s} = 13$ TeV via di-jet acoplanarity”, *JHEP* **05** (2024) 229, arXiv:2309.03788 [hep-ex].
- [80] **ATLAS** Collaboration, G. Aad *et al.*, “Strong Constraints on Jet Quenching in Centrality-Dependent p+Pb Collisions at 5.02 TeV from ATLAS”, *Phys. Rev. Lett.* **131** (2023) 072301, arXiv:2206.01138 [nucl-ex].
- [81] **ALICE** Collaboration, S. Acharya *et al.*, “Measurement of inclusive charged-particle jet production in pp and p–Pb collisions at $\sqrt{s_{\text{NN}}} = 5.02$ TeV”, *JHEP* **05** (2024) 041, arXiv:2307.10860 [nucl-ex].
- [82] **ALICE** Collaboration, S. Acharya *et al.*, “Measurement of inclusive charged-particle b-jet production in pp and p–Pb collisions at $\sqrt{s_{\text{NN}}} = 5.02$ TeV”, *JHEP* **01** (2022) 178, arXiv:2110.06104 [nucl-ex].
- [83] **ALICE** Collaboration, S. Acharya *et al.*, “Study of charged particle production at high p_{T} using event topology in pp, p–Pb and Pb–Pb collisions at $\sqrt{s_{\text{NN}}} = 5.02$ TeV”, *Phys. Lett. B* **843** (2023) 137649, arXiv:2204.10157 [nucl-ex].
- [84] **ALICE** Collaboration, K. Aamodt *et al.*, “The ALICE experiment at the CERN LHC”, *JINST* **3** (2008) S08002.
- [85] **ALICE** Collaboration, B. Abelev *et al.*, “Performance of the ALICE Experiment at the CERN LHC”, *Int. J. Mod. Phys. A* **29** (2014) 1430044, arXiv:1402.4476 [nucl-ex].
- [86] **ALICE** Collaboration, E. Abbas *et al.*, “Performance of the ALICE VZERO system”, *JINST* **8** (2013) P10016, arXiv:1306.3130 [nucl-ex].
- [87] **ALICE** Collaboration, K. Aamodt *et al.*, “Alignment of the ALICE Inner Tracking System with cosmic-ray tracks”, *JINST* **5** (2010) P03003, arXiv:1001.0502 [physics.ins-det].
- [88] J. Alme *et al.*, “The ALICE TPC, a large 3-dimensional tracking device with fast readout for ultra-high multiplicity events”, *Nucl. Instrum. Meth. A* **622** (2010) 316–367, arXiv:1001.1950 [physics.ins-det].
- [89] R. Santoro *et al.*, “The ALICE Silicon Pixel Detector: Readiness for the first proton beam”, *JINST* **4** (2009) P03023.
- [90] **ALICE** Collaboration, S. Acharya *et al.*, “Pseudorapidity densities of charged particles with transverse momentum thresholds in pp collisions at $\sqrt{s_{\text{NN}}} = 5.02$ and 13 TeV”, *Phys. Rev. D* **108** (2023) 072008, arXiv:2211.15364 [nucl-ex].

- [91] **ALICE** Collaboration, “ALICE 2016-2017-2018 luminosity determination for pp collisions at $\sqrt{s} = 13$ TeV”, *ALICE-PUBLIC-2021-005* (2021) . <https://cds.cern.ch/record/2776672>.
- [92] **ALICE** Collaboration, S. Acharya *et al.*, “Pseudorapidity distributions of charged particles as a function of mid- and forward rapidity multiplicities in pp collisions at $\sqrt{s} = 5.02, 7$ and 13 TeV”, *Eur. Phys. J. C* **81** (2021) 630, [arXiv:2009.09434](https://arxiv.org/abs/2009.09434) [nucl-ex].
- [93] **ALICE** Collaboration, S. Acharya *et al.*, “Transverse momentum spectra and nuclear modification factors of charged particles in pp, p–Pb and Pb–Pb collisions at the LHC”, *JHEP* **11** (2018) 013, [arXiv:1802.09145](https://arxiv.org/abs/1802.09145) [nucl-ex].
- [94] M. Ivanov, I. Belikov, P. Hristov, and K. Safarik, “Track reconstruction in high density environment”, *Nucl. Instrum. Meth. A* **566** (2006) 70–74.
- [95] **ALICE** Collaboration, “The ALICE definition of primary particles”, *ALICE-PUBLIC-2017-005* (2017) . <https://cds.cern.ch/record/2270008>.
- [96] G. I. Kopylov, “Like particle correlations as a tool to study the multiple production mechanism”, *Phys. Lett. B* **50** (1974) 472–474.
- [97] **ALICE** Collaboration, J. Adam *et al.*, “Anomalous evolution of the near-side jet peak shape in Pb–Pb collisions at $\sqrt{s_{NN}} = 2.76$ TeV”, *Phys. Rev. Lett.* **119** (2017) 102301, [arXiv:1609.06643](https://arxiv.org/abs/1609.06643) [nucl-ex].
- [98] R. Brun *et al.*, “GEANT: Detector Description and Simulation Tool; Oct 1994”, *CERN-W5013* (1993) . <http://cds.cern.ch/record/1082634>. Long Writeup W5013.
- [99] N. N. Ajitanand *et al.*, “Decomposition of harmonic and jet contributions to particle-pair correlations at ultra-relativistic energies”, *Phys. Rev.* **C72** (2005) 011902, [arXiv:nuc1-ex/0501025](https://arxiv.org/abs/nuc1-ex/0501025) [nucl-ex].
- [100] **ALICE** Collaboration, S. Acharya *et al.*, “Measurements of inclusive jet spectra in pp and central Pb-Pb collisions at $\sqrt{s_{NN}} = 5.02$ TeV”, *Phys. Rev. C* **101** (2020) 034911, [arXiv:1909.09718](https://arxiv.org/abs/1909.09718) [nucl-ex].
- [101] **ALICE** Collaboration, S. Acharya *et al.*, “Multiplicity dependence of charged-particle jet production in pp collisions at $\sqrt{s} = 13$ TeV”, *Eur. Phys. J. C* **82** (2022) 514, [arXiv:2202.01548](https://arxiv.org/abs/2202.01548) [nucl-ex].
- [102] **ALICE** Collaboration, S. Acharya *et al.*, “Multiplicity dependence of charged-particle intra-jet properties in pp collisions at $\sqrt{s} = 13$ TeV”, [arXiv:2311.13322](https://arxiv.org/abs/2311.13322) [hep-ex].
- [103] **ALICE** Collaboration, S. Acharya *et al.*, “Multiplicity dependence of light-flavor hadron production in pp collisions at $\sqrt{s} = 7$ TeV”, *Phys. Rev. C* **99** (2019) 024906, [arXiv:1807.11321](https://arxiv.org/abs/1807.11321) [nucl-ex].
- [104] R. Corke and T. Sjöstrand, “Interleaved Parton Showers and Tuning Prospects”, *JHEP* **03** (2011) 032, [arXiv:1011.1759](https://arxiv.org/abs/1011.1759) [hep-ph].
- [105] C. Bierlich, “Soft modifications to jet fragmentation in high energy proton–proton collisions”, *Phys. Lett. B* **795** (2019) 194–199, [arXiv:1901.07447](https://arxiv.org/abs/1901.07447) [hep-ph].
- [106] J. Kim, E.-J. Kim, S. Ji, and S. Lim, “Exploring the string shoving model in PYTHIA8 for collective behaviors in pp collisions”, *J. Korean Phys. Soc.* **79** (2021) 447–454, [arXiv:2108.09686](https://arxiv.org/abs/2108.09686) [nucl-th].

- [107] K. Werner, B. Guiot, I. Karpenko, and T. Pierog, “Analysing radial flow features in p–Pb and p–p collisions at several TeV by studying identified particle production in EPOS3”, *Phys. Rev. C* **89** (2014) 064903, arXiv:1312.1233 [nucl-th].
- [108] S. Bass *et al.*, “Microscopic models for ultrarelativistic heavy ion collisions”, *Prog. Part. Nucl. Phys.* **41** (1998) 255–369, arXiv:nucl-th/9803035.
- [109] M. Bleicher *et al.*, “Relativistic hadron-hadron collisions in the ultrarelativistic quantum molecular dynamics model”, *J. Phys. G* **25** (1999) 1859–1896, arXiv:hep-ph/9909407.
- [110] Z.-W. Lin, C. M. Ko, B.-A. Li, B. Zhang, and S. Pal, “A Multi-phase transport model for relativistic heavy ion collisions”, *Phys. Rev. C* **72** (2005) 064901, arXiv:nucl-th/0411110.
- [111] J. D. Orjuela Koop, A. Adare, D. McGlinchey, and J. L. Nagle, “Azimuthal anisotropy relative to the participant plane from a multiphase transport model in central p+Au, d+Au, and $^3\text{He} + \text{Au}$ collisions at $\sqrt{s_{\text{NN}}} = 200 \text{ GeV}$ ”, *Phys. Rev. C* **92** (2015) 054903, arXiv:1501.06880 [nucl-ex].
- [112] K. Gallmeister, H. Niemi, C. Greiner, and D. H. Rischke, “Exploring the applicability of dissipative fluid dynamics to small systems by comparison to the Boltzmann equation”, *Phys. Rev. C* **98** (2018) 024912, arXiv:1804.09512 [nucl-th].
- [113] A. Kurkela, U. A. Wiedemann, and B. Wu, “Flow in AA and pA as an interplay of fluid-like and non-fluid like excitations”, *Eur. Phys. J. C* **79** (2019) 965, arXiv:1905.05139 [hep-ph].
- [114] A. Kurkela, S. F. Taghavi, U. A. Wiedemann, and B. Wu, “Hydrodynamization in systems with detailed transverse profiles”, *Phys. Lett. B* **811** (2020) 135901, arXiv:2007.06851 [hep-ph].
- [115] V. E. Amrus, S. Schlichting, and C. Werthmann, “Development of transverse flow at small and large opacities in conformal kinetic theory”, *Phys. Rev. D* **105** (2022) 014031, arXiv:2109.03290 [hep-ph].
- [116] Y. Kanakubo, Y. Tachibana, and T. Hirano, “Nonequilibrium components in the region of very low transverse momentum in high-energy nuclear collisions”, *Phys. Rev. C* **106** (2022) 054908, arXiv:2207.13966 [nucl-th].
- [117] P. Romatschke, “Relativistic Fluid Dynamics Far From Local Equilibrium”, *Phys. Rev. Lett.* **120** (2018) 012301, arXiv:1704.08699 [hep-th].
- [118] A. Kurkela, A. Mazeliauskas, J.-F. Paquet, S. Schlichting, and D. Teaney, “Matching the Nonequilibrium Initial Stage of Heavy Ion Collisions to Hydrodynamics with QCD Kinetic Theory”, *Phys. Rev. Lett.* **122** (2019) 122302, arXiv:1805.01604 [hep-ph].
- [119] A. Kurkela, A. Mazeliauskas, J.-F. Paquet, S. Schlichting, and D. Teaney, “Effective kinetic description of event-by-event pre-equilibrium dynamics in high-energy heavy-ion collisions”, *Phys. Rev. C* **99** (2019) 034910, arXiv:1805.00961 [hep-ph].
- [120] A. Kurkela and A. Mazeliauskas, “Chemical Equilibration in Hadronic Collisions”, *Phys. Rev. Lett.* **122** (2019) 142301, arXiv:1811.03040 [hep-ph].
- [121] M. Strickland, “The non-equilibrium attractor for kinetic theory in relaxation time approximation”, *JHEP* **12** (2018) 128, arXiv:1809.01200 [nucl-th].
- [122] S. Kamata, M. Martinez, P. Plaschke, S. Ochsensfeld, and S. Schlichting, “Hydrodynamization and nonequilibrium Green’s functions in kinetic theory”, *Phys. Rev. D* **102** (2020) 056003, arXiv:2004.06751 [hep-ph].

A The ALICE Collaboration

S. Acharya ¹²⁷, A. Agarwal¹³⁵, G. Aglieri Rinella ³², L. Aglietta ²⁴, M. Agnello ²⁹, N. Agrawal ²⁵,
 Z. Ahammed ¹³⁵, S. Ahmad ¹⁵, S.U. Ahn ⁷¹, I. Ahuja ³⁷, A. Akindinov ¹⁴⁰, V. Akishina³⁸,
 M. Al-Turany ⁹⁷, D. Aleksandrov ¹⁴⁰, B. Alessandro ⁵⁶, H.M. Alfanda ⁶, R. Alfaro Molina ⁶⁷,
 B. Ali ¹⁵, A. Alici ²⁵, N. Alizadehvandchali ¹¹⁶, A. Alkin ¹⁰⁴, J. Alme ²⁰, G. Alocco ^{24,52}, T. Alt ⁶⁴,
 A.R. Altamura ⁵⁰, I. Altsybeev ⁹⁵, J.R. Alvarado ⁴⁴, C.O.R. Alvarez⁴⁴, M.N. Anaam ⁶, C. Andrei ⁴⁵,
 N. Andreou ¹¹⁵, A. Andronic ¹²⁶, E. Andronov ¹⁴⁰, V. Anguelov ⁹⁴, F. Antinori ⁵⁴, P. Antonioli ⁵¹,
 N. Apadula ⁷⁴, L. Aphecetche ¹⁰³, H. Appelshäuser ⁶⁴, C. Arata ⁷³, S. Arcelli ²⁵, R. Arnaldi ⁵⁶,
 J.G.M.C.A. Arneiro ¹¹⁰, I.C. Arsene ¹⁹, M. Arslanok ¹³⁸, A. Augustinus ³², R. Averbeck ⁹⁷,
 D. Averyanov ¹⁴⁰, M.D. Azmi ¹⁵, H. Baba¹²⁴, A. Badalà ⁵³, J. Bae ¹⁰⁴, Y.W. Baek ⁴⁰, X. Bai ¹²⁰,
 R. Bailhache ⁶⁴, Y. Bailung ⁴⁸, R. Bala ⁹¹, A. Balbino ²⁹, A. Baldisseri ¹³⁰, B. Balis ², Z. Banoo ⁹¹,
 V. Barbasova³⁷, F. Barile ³¹, L. Barioglio ⁵⁶, M. Barlou⁷⁸, B. Barman⁴¹, G.G. Barnaföldi ⁴⁶,
 L.S. Barnby ¹¹⁵, E. Barreau ¹⁰³, V. Barret ¹²⁷, L. Barreto ¹¹⁰, C. Bartels ¹¹⁹, K. Barth ³²,
 E. Bartsch ⁶⁴, N. Bastid ¹²⁷, S. Basu ⁷⁵, G. Batigne ¹⁰³, D. Battistini ⁹⁵, B. Batyunya ¹⁴¹, D. Bauri⁴⁷,
 J.L. Bazo Alba ¹⁰¹, I.G. Bearden ⁸³, C. Beattie ¹³⁸, P. Becht ⁹⁷, D. Behera ⁴⁸, I. Belikov ¹²⁹,
 A.D.C. Bell Hechavarria ¹²⁶, F. Bellini ²⁵, R. Bellwied ¹¹⁶, S. Belokurova ¹⁴⁰, L.G.E. Beltran ¹⁰⁹,
 Y.A.V. Beltran ⁴⁴, G. Bencedi ⁴⁶, A. Bensaoula¹¹⁶, S. Beole ²⁴, Y. Berdnikov ¹⁴⁰, A. Berdnikova ⁹⁴,
 L. Bergmann ⁹⁴, M.G. Besoiu ⁶³, L. Betev ³², P.P. Bhaduri ¹³⁵, A. Bhasin ⁹¹, B. Bhattacharjee ⁴¹,
 L. Bianchi ²⁴, J. Bielčík ³⁵, J. Bielčíková⁸⁶, A.P. Bigot ¹²⁹, A. Bilandzic ⁹⁵, G. Biro ⁴⁶, S. Biswas ⁴,
 N. Bize ¹⁰³, J.T. Blair ¹⁰⁸, D. Blau ¹⁴⁰, M.B. Blidaru ⁹⁷, N. Bluhme³⁸, C. Blume ⁶⁴, G. Boca ^{21,55},
 F. Bock ⁸⁷, T. Bodova ²⁰, J. Bok ¹⁶, L. Boldizsár ⁴⁶, M. Bombara ³⁷, P.M. Bond ³², G. Bonomi ^{134,55},
 H. Borel ¹³⁰, A. Borissov ¹⁴⁰, A.G. Borquez Carcamo ⁹⁴, E. Botta ²⁴, Y.E.M. Bouziani ⁶⁴,
 L. Bratrud ⁶⁴, P. Braun-Munzinger ⁹⁷, M. Bregant ¹¹⁰, M. Broz ³⁵, G.E. Bruno ^{96,31},
 V.D. Buchakchiev ³⁶, M.D. Buckland ⁸⁵, D. Budnikov ¹⁴⁰, H. Buesching ⁶⁴, S. Bufalino ²⁹,
 P. Buhler ¹⁰², N. Burmasov ¹⁴⁰, Z. Buthelezi ^{68,123}, A. Bylinkin ²⁰, S.A. Bysiak¹⁰⁷, J.C. Cabanillas
 Noris ¹⁰⁹, M.F.T. Cabrera¹¹⁶, M. Cai ⁶, H. Caines ¹³⁸, A. Caliva ²⁸, E. Calvo Villar ¹⁰¹,
 J.M.M. Camacho ¹⁰⁹, P. Camerini ²³, F.D.M. Canedo ¹¹⁰, S.L. Cantway ¹³⁸, M. Carabas ¹¹³,
 A.A. Carballo ³², F. Carnesecchi ³², R. Caron ¹²⁸, L.A.D. Carvalho ¹¹⁰, J. Castillo Castellanos ¹³⁰,
 M. Castoldi ³², F. Catalano ³², S. Cattaruzzi ²³, C. Ceballos Sanchez ⁷, R. Cerri ²⁴, I. Chakaberia ⁷⁴,
 P. Chakraborty ¹³⁶, S. Chandra ¹³⁵, S. Chapeland ³², M. Chartier ¹¹⁹, S. Chattopadhyay¹³⁵,
 S. Chattopadhyay ¹³⁵, S. Chattopadhyay ⁹⁹, M. Chen³⁹, T. Cheng ⁶, C. Cheshkov ¹²⁸, V. Chibante
 Barroso ³², D.D. Chinellato ¹⁰², E.S. Chizzali ^{II,95}, J. Cho ⁵⁸, S. Cho ⁵⁸, P. Chochula ³²,
 Z.A. Chochulska¹³⁶, D. Choudhury⁴¹, P. Christakoglou ⁸⁴, C.H. Christensen ⁸³, P. Christiansen ⁷⁵,
 T. Chujo ¹²⁵, M. Ciacco ²⁹, C. Cicalo ⁵², M.R. Ciupek ⁹⁷, G. Clai^{III,51}, F. Colamaria ⁵⁰, J.S. Colburn¹⁰⁰,
 D. Colella ³¹, A. Colelli³¹, M. Colocci ²⁵, M. Concas ³², G. Conesa Balbastre ⁷³, Z. Conesa del
 Valle ¹³¹, G. Contin ²³, J.G. Contreras ³⁵, M.L. Coquet ¹⁰³, P. Cortese ^{133,56}, M.R. Cosentino ¹¹²,
 F. Costa ³², S. Costanza ^{21,55}, C. Cot ¹³¹, P. Crochet ¹²⁷, R. Cruz-Torres ⁷⁴, M.M. Czarnynoga¹³⁶,
 A. Dainese ⁵⁴, G. Dange³⁸, M.C. Danisch ⁹⁴, A. Danu ⁶³, P. Das ⁸⁰, S. Das ⁴, A.R. Dash ¹²⁶,
 S. Dash ⁴⁷, A. De Caro ²⁸, G. de Cataldo ⁵⁰, J. de Cuveland³⁸, A. De Falco ²², D. De Gruttola ²⁸, N. De
 Marco ⁵⁶, C. De Martin ²³, S. De Pasquale ²⁸, R. Deb ¹³⁴, R. Del Grande ⁹⁵, L. Dello Stritto ³²,
 W. Deng ⁶, K.C. Devereaux¹⁸, P. Dhankher ¹⁸, D. Di Bari ³¹, A. Di Mauro ³², B. Di Ruzza ¹³²,
 B. Diab ¹³⁰, R.A. Diaz ^{141,7}, T. Dietel ¹¹⁴, Y. Ding ⁶, J. Ditzel ⁶⁴, R. Divià ³², Ø. Djuvsland²⁰,
 U. Dmitrieva ¹⁴⁰, A. Dobrin ⁶³, B. Dönigus ⁶⁴, J.M. Dubinski ¹³⁶, A. Dubla ⁹⁷, P. Dupieux ¹²⁷,
 N. Dzalaiova¹³, T.M. Eder ¹²⁶, R.J. Ehlers ⁷⁴, F. Eisenhut ⁶⁴, R. Ejima ⁹², D. Elia ⁵⁰, B. Erazmus ¹⁰³,
 F. Ercolessi ²⁵, B. Espagnon ¹³¹, G. Eulisse ³², D. Evans ¹⁰⁰, S. Evdokimov ¹⁴⁰, L. Fabbietti ⁹⁵,
 M. Faggin ²³, J. Faivre ⁷³, F. Fan ⁶, W. Fan ⁷⁴, A. Fantoni ⁴⁹, M. Fasel ⁸⁷, A. Feliciello ⁵⁶,
 G. Feofilov ¹⁴⁰, A. Fernández Téllez ⁴⁴, L. Ferrandi ¹¹⁰, M.B. Ferrer ³², A. Ferrero ¹³⁰,
 C. Ferrero ^{IV,56}, A. Ferretti ²⁴, V.J.G. Feuillard ⁹⁴, V. Filova ³⁵, D. Finogeev ¹⁴⁰, F.M. Fionda ⁵²,
 E. Flatland³², F. Flor ^{138,116}, A.N. Flores ¹⁰⁸, S. Foertsch ⁶⁸, I. Fokin ⁹⁴, S. Fokin ¹⁴⁰, U. Follo ^{IV,56},
 E. Fragiaco ⁵⁷, E. Frajna ⁴⁶, U. Fuchs ³², N. Funicello ²⁸, C. Furget ⁷³, A. Furs ¹⁴⁰,
 T. Fusayasu ⁹⁸, J.J. Gaardhøje ⁸³, M. Gagliardi ²⁴, A.M. Gago ¹⁰¹, T. Gahlaut⁴⁷, C.D. Galvan ¹⁰⁹,
 S. Gami⁸⁰, D.R. Gangadharan ¹¹⁶, P. Ganoti ⁷⁸, C. Garabatos ⁹⁷, J.M. García ⁴⁴, T. García Chávez ⁴⁴,
 E. García-Solis ⁹, C. Gargiulo ³², P. Gasik ⁹⁷, H.M. Gaur³⁸, A. Gautam ¹¹⁸, M.B. Gay Ducati ⁶⁶,
 M. Germain ¹⁰³, R.A. Gernhaeuser⁹⁵, C. Ghosh¹³⁵, M. Giacalone ⁵¹, G. Gioachin ²⁹, S.K. Giri¹³⁵,
 P. Giubellino ^{97,56}, P. Giubilato ²⁷, A.M.C. Glaenger

L.K. Graczykowski ¹³⁶, E. Grecka ⁸⁶, A. Grelli ⁵⁹, C. Grigoras ³², V. Grigoriev ¹⁴⁰, S. Grigoryan ^{141,1},
 F. Groso ³², J.F. Grosse-Oetringhaus ³², R. Grosso ⁹⁷, D. Grund ³⁵, N.A. Grunwald⁹⁴,
 G.G. Guardiano ¹¹¹, R. Guernane ⁷³, M. Guilbaud ¹⁰³, K. Gulbrandsen ⁸³, J.J.W.K. Gumprecht¹⁰²,
 T. Gündem ⁶⁴, T. Gunji ¹²⁴, W. Guo ⁶, A. Gupta ⁹¹, R. Gupta ⁹¹, R. Gupta ⁴⁸, K. Gwizdziel ¹³⁶,
 L. Gyulai ⁴⁶, C. Hadjidakis ¹³¹, F.U. Haider ⁹¹, S. Haidlova ³⁵, M. Haldar⁴, H. Hamagaki ⁷⁶,
 Y. Han ¹³⁹, B.G. Hanley ¹³⁷, R. Hannigan ¹⁰⁸, J. Hansen ⁷⁵, M.R. Haque ⁹⁷, J.W. Harris ¹³⁸,
 A. Harton ⁹, M.V. Hartung ⁶⁴, H. Hassan ¹¹⁷, D. Hatzifotiadou ⁵¹, P. Hauer ⁴², L.B. Havener ¹³⁸,
 E. Hellbär ³², H. Helstrup ³⁴, M. Hemmer ⁶⁴, T. Herman ³⁵, S.G. Hernandez¹¹⁶, G. Herrera Corral ⁸,
 S. Herrmann ¹²⁸, K.F. Hetland ³⁴, B. Heybeck ⁶⁴, H. Hillemanns ³², B. Hippolyte ¹²⁹, I.P.M. Hobus⁸⁴,
 F.W. Hoffmann ⁷⁰, B. Hofman ⁵⁹, G.H. Hong ¹³⁹, M. Horst ⁹⁵, A. Horzyk ², Y. Hou ⁶, P. Hristov ³²,
 P. Huhn⁶⁴, L.M. Huhta ¹¹⁷, T.J. Humanic ⁸⁸, A. Hutson ¹¹⁶, D. Hutter ³⁸, M.C. Hwang ¹⁸, R. Ilkaev¹⁴⁰,
 M. Inaba ¹²⁵, G.M. Innocenti ³², M. Ippolitov ¹⁴⁰, A. Isakov ⁸⁴, T. Isidori ¹¹⁸, M.S. Islam ⁹⁹,
 S. Iurchenko¹⁴⁰, M. Ivanov ⁹⁷, M. Ivanov¹³, V. Ivanov ¹⁴⁰, K.E. Iversen ⁷⁵, M. Jablonski ²,
 B. Jacak ^{18,74}, N. Jacazio ²⁵, P.M. Jacobs ⁷⁴, S. Jadlovská¹⁰⁶, J. Jadlovsky¹⁰⁶, S. Jaelani ⁸², C. Jahnke ¹¹⁰,
 M.J. Jakubowska ¹³⁶, M.A. Janik ¹³⁶, T. Janson⁷⁰, S. Ji ¹⁶, S. Jia ¹⁰, T. Jiang ¹⁰, A.A.P. Jimenez ⁶⁵,
 F. Jonas ⁷⁴, D.M. Jones ¹¹⁹, J.M. Jowett ^{32,97}, J. Jung ⁶⁴, M. Jung ⁶⁴, A. Junique ³², A. Jusko ¹⁰⁰,
 J. Kaewjai¹⁰⁵, P. Kalinak ⁶⁰, A. Kalweit ³², A. Karasu Uysal ^{V,72}, D. Karatovic ⁸⁹, N. Karatzenis¹⁰⁰,
 O. Karavichev ¹⁴⁰, T. Karavicheva ¹⁴⁰, E. Karpechev ¹⁴⁰, M.J. Karwowska ^{32,136}, U. Kebschull ⁷⁰,
 M. Keil ³², B. Ketzer ⁴², J. Keul ⁶⁴, S.S. Khade ⁴⁸, A.M. Khan ¹²⁰, S. Khan ¹⁵, A. Khanzadeev ¹⁴⁰,
 Y. Kharlov ¹⁴⁰, A. Khatun ¹¹⁸, A. Khuntia ³⁵, Z. Khuranova ⁶⁴, B. Kileng ³⁴, B. Kim ¹⁰⁴, C. Kim ¹⁶,
 D.J. Kim ¹¹⁷, E.J. Kim ⁶⁹, J. Kim ¹³⁹, J. Kim ⁵⁸, J. Kim ^{32,69}, M. Kim ¹⁸, S. Kim ¹⁷, T. Kim ¹³⁹,
 K. Kimura ⁹², A. Kirkova³⁶, S. Kirsch ⁶⁴, I. Kisel ³⁸, S. Kiselev ¹⁴⁰, A. Kisiel ¹³⁶, J.P. Kitowski ²,
 J.L. Klay ⁵, J. Klein ³², S. Klein ⁷⁴, C. Klein-Bösing ¹²⁶, M. Kleiner ⁶⁴, T. Klemenz ⁹⁵, A. Kluge ³²,
 C. Kobdaj ¹⁰⁵, R. Kohara¹²⁴, T. Kollegger⁹⁷, A. Kondratyev ¹⁴¹, N. Kondratyeva ¹⁴⁰, J. König ⁶⁴,
 S.A. Konigstorfer ⁹⁵, P.J. Konopka ³², G. Kornakov ¹³⁶, M. Korwieser ⁹⁵, S.D. Koryciak ², C. Koster⁸⁴,
 A. Kotliarov ⁸⁶, N. Kovacic⁸⁹, V. Kovalenko ¹⁴⁰, M. Kowalski ¹⁰⁷, V. Kozuharov ³⁶, G. Kozlov³⁸,
 I. Králik ⁶⁰, A. Kravčáková ³⁷, L. Krcal ^{32,38}, M. Krivda ^{100,60}, F. Krizek ⁸⁶, K. Krizkova Gajdosova ³²,
 C. Krug ⁶⁶, M. Krüger ⁶⁴, D.M. Krupova ³⁵, E. Kryshen ¹⁴⁰, V. Kučera ⁵⁸, C. Kuhn ¹²⁹,
 P.G. Kuijjer ⁸⁴, T. Kumaoka¹²⁵, D. Kumar¹³⁵, L. Kumar ⁹⁰, N. Kumar⁹⁰, S. Kumar ⁵⁰, S. Kundu ³²,
 P. Kurashvili ⁷⁹, A. Kurepin ¹⁴⁰, A.B. Kurepin ¹⁴⁰, A. Kuryakin ¹⁴⁰, S. Kushpil ⁸⁶, V. Kuskov ¹⁴⁰,
 M. Kutyla¹³⁶, A. Kuznetsov¹⁴¹, M.J. Kweon ⁵⁸, Y. Kwon ¹³⁹, S.L. La Pointe ³⁸, P. La Rocca ²⁶,
 A. Lakrathok¹⁰⁵, M. Lamanna ³², A.R. Landou ⁷³, R. Langoy ¹²¹, P. Larionov ³², E. Laudi ³²,
 L. Lautner ^{32,95}, R.A.N. Laveaga¹⁰⁹, R. Lavicka ¹⁰², R. Lea ^{134,55}, H. Lee ¹⁰⁴, I. Legrand ⁴⁵,
 G. Legras ¹²⁶, J. Lehrbach ³⁸, A.M. Lejeune³⁵, T.M. Lelek², R.C. Lemmon ^{I,85}, I. León Monzón ¹⁰⁹,
 M.M. Lesch ⁹⁵, E.D. Lesser ¹⁸, P. Lévai ⁴⁶, M. Li⁶, P. Li¹⁰, X. Li¹⁰, B.E. Liang-gilman ¹⁸, J. Lien ¹²¹,
 R. Lietava ¹⁰⁰, I. Likmeta ¹¹⁶, B. Lim ²⁴, S.H. Lim ¹⁶, V. Lindenstruth ³⁸, C. Lippmann ⁹⁷,
 D.H. Liu ⁶, J. Liu ¹¹⁹, G.S.S. Liveraro ¹¹¹, I.M. Lofnes ²⁰, C. Loizides ⁸⁷, S. Lokos ¹⁰⁷, J. Lömker ⁵⁹,
 X. Lopez ¹²⁷, E. López Torres ⁷, C. Lotteau¹²⁸, P. Lu ^{97,120}, Z. Lu ¹⁰, F.V. Lugo ⁶⁷, J.R. Luhder ¹²⁶,
 M. Lunardon ²⁷, G. Luparello ⁵⁷, Y.G. Ma ³⁹, M. Mager ³², A. Maire ¹²⁹, E.M. Majerz²,
 M.V. Makariev ³⁶, M. Malaev ¹⁴⁰, G. Malfattore ²⁵, N.M. Malik ⁹¹, S.K. Malik ⁹¹,
 L. Malinina ^{I,VIII,141}, D. Mallick ¹³¹, N. Mallick ⁴⁸, G. Mandaglio ^{30,53}, S.K. Mandal ⁷⁹, A. Manea ⁶³,
 V. Manko ¹⁴⁰, F. Manso ¹²⁷, V. Manzari ⁵⁰, Y. Mao ⁶, R.W. Marcjan ², G.V. Margagliotti ²³,
 A. Margotti ⁵¹, A. Marín ⁹⁷, C. Markert ¹⁰⁸, C.F.B. Marquez³¹, P. Martinengo ³², M.I. Martínez ⁴⁴,
 G. Martínez García ¹⁰³, M.P.P. Martins ¹¹⁰, S. Masciocchi ⁹⁷, M. Maserà ²⁴, A. Masoni ⁵²,
 L. Massacrier ¹³¹, O. Massen ⁵⁹, A. Mastroserio ^{132,50}, O. Matonoha ⁷⁵, S. Mattiazzo ²⁷, A. Matyja ¹⁰⁷,
 F. Mazzaschi ^{32,24}, M. Mazzilli ¹¹⁶, Y. Melikyan ⁴³, M. Melo ¹¹⁰, A. Menchaca-Rocha ⁶⁷,
 J.E.M. Mendez ⁶⁵, E. Meninno ¹⁰², A.S. Menon ¹¹⁶, M.W. Menzel^{32,94}, M. Meres ¹³, Y. Miake¹²⁵,
 L. Micheletti ³², D. Mihai¹¹³, D.L. Mihaylov ⁹⁵, K. Mikhaylov ^{141,140}, N. Minafra ¹¹⁸, D. Miśkowiec ⁹⁷,
 A. Modak ¹³⁴, B. Mohanty⁸⁰, M. Mohisin Khan ^{VI,15}, M.A. Molander ⁴³, S. Monira ¹³⁶,
 C. Mordasini ¹¹⁷, D.A. Moreira De Godoy ¹²⁶, I. Morozov ¹⁴⁰, A. Morsch ³², T. Mrnjavac ³²,
 V. Muccifora ⁴⁹, S. Muhuri ¹³⁵, J.D. Mulligan ⁷⁴, A. Mulliri ²², M.G. Munhoz ¹¹⁰, R.H. Munzer ⁶⁴,
 H. Murakami ¹²⁴, S. Murray ¹¹⁴, L. Musa ³², J. Musinsky ⁶⁰, J.W. Myrcha ¹³⁶, B. Naik ¹²³,
 A.I. Nambrath ¹⁸, B.K. Nandi ⁴⁷, R. Nania ⁵¹, E. Nappi ⁵⁰, A.F. Nassirpour

J. Norman ¹¹⁹, N. Novitzky ⁸⁷, P. Nowakowski ¹³⁶, A. Nyanin ¹⁴⁰, J. Nystrand ²⁰, S. Oh ¹⁷,
A. Ohlson ⁷⁵, V.A. Okorokov ¹⁴⁰, J. Oleniacz ¹³⁶, A. Onnerstad ¹¹⁷, C. Oppedisano ⁵⁶, A. Ortiz
Velasquez ⁶⁵, J. Otwinowski ¹⁰⁷, M. Oya ⁹², K. Oyama ⁷⁶, Y. Pachmayer ⁹⁴, S. Padhan ⁴⁷,
D. Pagano ^{134,55}, G. Paic ⁶⁵, S. Paisano-Guzmán ⁴⁴, A. Palasciano ⁵⁰, I. Panasenkov ⁷⁵, S. Panebianco ¹³⁰,
C. Pantouvakis ²⁷, H. Park ¹²⁵, H. Park ¹⁰⁴, J. Park ¹²⁵, J.E. Parkkila ³², Y. Patley ⁴⁷, R.N. Patra ⁵⁰,
B. Paul ¹³⁵, H. Pei ⁶, T. Peitzmann ⁵⁹, X. Peng ¹¹, M. Pennisi ²⁴, S. Perciballi ²⁴, D. Peresunko ¹⁴⁰,
G.M. Perez ⁷, Y. Pestov ¹⁴⁰, M.T. Petersen ⁸³, V. Petrov ¹⁴⁰, M. Petrovici ⁴⁵, S. Piano ⁵⁷, M. Pikna ¹³,
P. Pillot ¹⁰³, O. Pinazza ^{51,32}, L. Pinsky ¹¹⁶, C. Pinto ⁹⁵, S. Pisano ⁴⁹, M. Płoskoń ⁷⁴, M. Planinic ⁸⁹,
F. Pliquett ⁶⁴, D.K. Plociennik ², M.G. Poghosyan ⁸⁷, B. Polichtchouk ¹⁴⁰, S. Politano ²⁹, N. Poljak ⁸⁹,
A. Pop ⁴⁵, S. Porteboeuf-Houssais ¹²⁷, V. Pozdniakov ^{1,141}, I.Y. Pozos ⁴⁴, K.K. Pradhan ⁴⁸,
S.K. Prasad ⁴, S. Prasad ⁴⁸, R. Preghenella ⁵¹, F. Prino ⁵⁶, C.A. Pruneau ¹³⁷, I. Pshenichnov ¹⁴⁰,
M. Puccio ³², S. Pucillo ²⁴, S. Qiu ⁸⁴, L. Quaglia ²⁴, A.M.K. Radhakrishnan ⁴⁸, S. Ragoni ¹⁴,
A. Rai ¹³⁸, A. Rakotozafindrabe ¹³⁰, L. Ramello ^{133,56}, F. Rami ¹²⁹, M. Rasa ²⁶, S.S. Räsänen ⁴³,
R. Rath ⁵¹, M.P. Rauch ²⁰, I. Ravasenga ³², K.F. Read ^{87,122}, C. Reckziegel ¹¹², A.R. Redelbach ³⁸,
K. Redlich ^{VII,79}, C.A. Reetz ⁹⁷, H.D. Regules-Medel ⁴⁴, A. Rehman ²⁰, F. Reidt ³², H.A. Reme-Ness ³⁴,
K. Reygiers ⁹⁴, A. Riabov ¹⁴⁰, V. Riabov ¹⁴⁰, R. Ricci ²⁸, M. Richter ²⁰, A.A. Riedel ⁹⁵,
W. Riegler ³², A.G. Riffero ²⁴, M. Rignanese ²⁷, C. Ripoli ²⁸, C. Ristea ⁶³, M.V. Rodriguez ³²,
M. Rodríguez Cahuantzi ⁴⁴, S.A. Rodríguez Ramírez ⁴⁴, K. Røed ¹⁹, R. Rogalev ¹⁴⁰, E. Rogochaya ¹⁴¹,
T.S. Rogoschinski ⁶⁴, D. Rohr ³², D. Röhrich ²⁰, S. Rojas Torres ³⁵, P.S. Rokita ¹³⁶, G. Romanenko ²⁵,
F. Ronchetti ³², E.D. Rosas ⁶⁵, K. Roslon ¹³⁶, A. Rossi ⁵⁴, A. Roy ⁴⁸, S. Roy ⁴⁷, N. Rubini ^{51,25},
J.A. Rudolph ⁸⁴, D. Ruggiano ¹³⁶, R. Rui ²³, P.G. Russek ², R. Russo ⁸⁴, A. Rustamov ⁸¹,
E. Ryabinkin ¹⁴⁰, Y. Ryabov ¹⁴⁰, A. Rybicki ¹⁰⁷, J. Ryu ¹⁶, W. Rzesza ¹³⁶, B. Sabiu ⁵¹, S. Sadovsky ¹⁴⁰,
J. Saetre ²⁰, K. Šafařík ³⁵, S. Saha ⁸⁰, B. Sahoo ⁴⁸, R. Sahoo ⁴⁸, S. Sahoo ⁶¹, D. Sahu ⁴⁸, P.K. Sahu ⁶¹,
J. Saini ¹³⁵, K. Sajdakova ³⁷, S. Sakai ¹²⁵, M.P. Salvan ⁹⁷, S. Sambyal ⁹¹, D. Samitz ¹⁰², I. Sanna ^{32,95},
T.B. Saramela ¹¹⁰, D. Sarkar ⁸³, P. Sarma ⁴¹, V. Sarritzu ²², V.M. Sarti ⁹⁵, M.H.P. Sas ³², S. Sawan ⁸⁰,
E. Scapparone ⁵¹, J. Schambach ⁸⁷, H.S. Scheid ⁶⁴, C. Schiaua ⁴⁵, R. Schicker ⁹⁴, F. Schlepfer ⁹⁴,
A. Schmah ⁹⁷, C. Schmidt ⁹⁷, H.R. Schmidt ⁹³, M.O. Schmidt ³², M. Schmidt ⁹³, N.V. Schmidt ⁸⁷,
A.R. Schmier ¹²², R. Schotter ^{102,129}, A. Schröter ³⁸, J. Schukraft ³², K. Schweda ⁹⁷, G. Scioli ²⁵,
E. Scomparin ⁵⁶, J.E. Seger ¹⁴, Y. Sekiguchi ¹²⁴, D. Sekihata ¹²⁴, M. Selina ⁸⁴, I. Selyuzhenkov ⁹⁷,
S. Senyukov ¹²⁹, J.J. Seo ⁹⁴, D. Serebryakov ¹⁴⁰, L. Serkin ⁶⁵, L. Šerkšnytė ⁹⁵, A. Sevcenco ⁶³,
T.J. Shaba ⁶⁸, A. Shabetai ¹⁰³, R. Shahoyan ³², A. Shangaraev ¹⁴⁰, B. Sharma ⁹¹, D. Sharma ⁴⁷,
H. Sharma ⁵⁴, M. Sharma ⁹¹, S. Sharma ⁷⁶, S. Sharma ⁹¹, U. Sharma ⁹¹, A. Shatat ¹³¹, O. Sheibani ¹¹⁶,
K. Shigaki ⁹², M. Shimomura ⁷⁷, J. Shin ¹², S. Shirinkin ¹⁴⁰, Q. Shou ³⁹, Y. Sibiriak ¹⁴⁰, S. Siddhanta ⁵²,
T. Siemiarczuk ⁷⁹, T.F. Silva ¹¹⁰, D. Silvermyr ⁷⁵, T. Simantathammakul ¹⁰⁵, R. Simeonov ³⁶, B. Singh ⁹¹,
B. Singh ⁹⁵, K. Singh ⁴⁸, R. Singh ⁸⁰, R. Singh ⁹¹, R. Singh ⁹⁷, S. Singh ¹⁵, V.K. Singh ¹³⁵,
V. Singhal ¹³⁵, T. Sinha ⁹⁹, B. Sitar ¹³, M. Sitta ^{133,56}, T.B. Skaali ¹⁹, G. Skorodumovs ⁹⁴,
N. Smirnov ¹³⁸, R.J.M. Snellings ⁵⁹, E.H. Solheim ¹⁹, J. Song ¹⁶, C. Sonnabend ^{32,97},
J.M. Sonneveld ⁸⁴, F. Soramel ²⁷, A.B. Soto-herandez ⁸⁸, R. Spijkers ⁸⁴, I. Sputowska ¹⁰⁷, J. Staa ⁷⁵,
J. Stachel ⁹⁴, I. Stan ⁶³, P.J. Steffanic ¹²², T. Stellhorn ¹²⁶, S.F. Stiefelmaier ⁹⁴, D. Stocco ¹⁰³,
I. Storehaug ¹⁹, N.J. Strangmann ⁶⁴, P. Stratmann ¹²⁶, S. Strazzi ²⁵, A. Sturniolo ^{30,53}, C.P. Stylianidis ⁸⁴,
A.A.P. Suaide ¹¹⁰, C. Suire ¹³¹, M. Sukhanov ¹⁴⁰, M. Suljic ³², R. Sultanov ¹⁴⁰, V. Sumberia ⁹¹,
S. Sumowidagdo ⁸², M. Szymkowski ¹³⁶, S.F. Taghavi ⁹⁵, G. Taillepied ⁹⁷, J. Takahashi ¹¹¹,
G.J. Tambave ⁸⁰, S. Tang ⁶, Z. Tang ¹²⁰, J.D. Tapia Takaki ¹¹⁸, N. Tapus ¹¹³, L.A. Tarasovicova ³⁷,
M.G. Tarzila ⁴⁵, G.F. Tassielli ³¹, A. Tauro ³², A. Távira García ¹³¹, G. Tejeda Muñoz ⁴⁴, L. Terlizzi ²⁴,
C. Terrevoli ⁵⁰, S. Thakur ⁴, D. Thomas ¹⁰⁸, A. Tikhonov ¹⁴⁰, N. Tiltmann ^{32,126}, A.R. Timmins ¹¹⁶,
M. Tkacik ¹⁰⁶, T. Tkacik ¹⁰⁶, A. Toia ⁶⁴, R. Tokumoto ⁹², S. Tomassini ²⁵, K. Tomohiro ⁹², N. Topilskaya ¹⁴⁰,
M. Toppi ⁴⁹, V.V. Torres ¹⁰³, A.G. Torres Ramos ³¹, A. Trifiro ^{30,53}, T. Triloki ⁹⁶, A.S. Triolo ^{32,30,53},
S. Tripathy ³², T. Tripathy ⁴⁷, S. Trogolo ²⁴, V. Trubnikov ³, W.H. Trzaska ¹¹⁷, T.P. Trzcinski ¹³⁶,
C. Tzolanta ¹⁹, R. Tu ³⁹, A. Tumkin ¹⁴⁰, R. Turrisi ⁵⁴, T.S. Tveter ¹⁹, K. Ullaland ²⁰, B. Ulukutlu ⁹⁵,
S. Upadhyaya ¹⁰⁷, A. Uras ¹²⁸, M. Urioni ¹³⁴, G.L. Usai ²², M. Vala ³⁷, N. Valle ⁵⁵, L.V.R. van
Doremalen ⁵⁹, M. van Leeuwen ⁸⁴, C.A. van Veen ⁹⁴, R.J.G. van Weelden ⁸⁴, P. Vande Vyvre ³²,
D. Varga ⁴⁶, Z. Varga ⁴⁶, P. Vargas Torres ⁶⁵, M. Vasileiou ⁷⁸, A. Vasiliev ^{1,140}, O. Vázquez Doce ⁴⁹,
O. Vazquez Rueda ¹¹⁶, V. Vechernin ¹⁴⁰, E. Vercellin ²⁴, S. Vergara Limón ⁴⁴, R. Verma ⁴⁷,
L. Vermunt ⁹⁷, R. Vértesi ⁴⁶, M. Verweij ⁵⁹, L. Vickovic ³³, Z. Vilakazi ¹²³, O. Villalobos Baillie ¹⁰⁰,
A. Villani ²³, A. Vinogradov ¹⁴⁰, T. Virgili ²⁸, M.M.O. Virta ¹¹⁷, A. Vodopyanov ¹⁴¹, B. Volkel ³²,
M.A. Völkl ⁹⁴, S.A. Voloshin ¹³⁷, G. Volpe ³¹, B. von Haller ³², I. Vorobyev ³², N. Vozniuk ¹⁴⁰,

J. Vrláková³⁷, J. Wan³⁹, C. Wang³⁹, D. Wang³⁹, Y. Wang³⁹, Y. Wang⁶, Z. Wang³⁹,
 A. Wegrzynek³², F.T. Weiglhofer³⁸, S.C. Wenzel³², J.P. Wessels¹²⁶, J. Wiechula⁶⁴, J. Wikne¹⁹,
 G. Wilk⁷⁹, J. Wilkinson⁹⁷, G.A. Willems¹²⁶, B. Windelband⁹⁴, M. Winn¹³⁰, J.R. Wright¹⁰⁸,
 W. Wu³⁹, Y. Wu¹²⁰, Z. Xiong¹²⁰, R. Xu⁶, A. Yadav⁴², A.K. Yadav¹³⁵, Y. Yamaguchi⁹², S. Yang²⁰,
 S. Yano⁹², E.R. Yeats¹⁸, Z. Yin⁶, I.-K. Yoo¹⁶, J.H. Yoon⁵⁸, H. Yu¹², S. Yuan²⁰, A. Yuncu⁹⁴,
 V. Zaccolo²³, C. Zampolli³², F. Zanone⁹⁴, N. Zardoshti³², A. Zarochentsev¹⁴⁰, P. Závada⁶²,
 N. Zaviyalov¹⁴⁰, M. Zhalov¹⁴⁰, B. Zhang^{94,6}, C. Zhang¹³⁰, L. Zhang³⁹, M. Zhang^{127,6}, M. Zhang⁶,
 S. Zhang³⁹, X. Zhang⁶, Y. Zhang¹²⁰, Z. Zhang⁶, M. Zhao¹⁰, V. Zhrebchevskii¹⁴⁰, Y. Zhi¹⁰,
 D. Zhou⁶, Y. Zhou⁸³, J. Zhu^{54,6}, S. Zhu¹²⁰, Y. Zhu⁶, S.C. Zugravel⁵⁶, N. Zurlo^{134,55}

Affiliation Notes

^I Deceased

^{II} Also at: Max-Planck-Institut für Physik, Munich, Germany

^{III} Also at: Italian National Agency for New Technologies, Energy and Sustainable Economic Development (ENEA), Bologna, Italy

^{IV} Also at: Dipartimento DET del Politecnico di Torino, Turin, Italy

^V Also at: Yildiz Technical University, Istanbul, Türkiye

^{VI} Also at: Department of Applied Physics, Aligarh Muslim University, Aligarh, India

^{VII} Also at: Institute of Theoretical Physics, University of Wrocław, Poland

^{VIII} Also at: An institution covered by a cooperation agreement with CERN

Collaboration Institutes

¹ A.I. Alikhanyan National Science Laboratory (Yerevan Physics Institute) Foundation, Yerevan, Armenia

² AGH University of Krakow, Cracow, Poland

³ Bogolyubov Institute for Theoretical Physics, National Academy of Sciences of Ukraine, Kiev, Ukraine

⁴ Bose Institute, Department of Physics and Centre for Astroparticle Physics and Space Science (CAPSS), Kolkata, India

⁵ California Polytechnic State University, San Luis Obispo, California, United States

⁶ Central China Normal University, Wuhan, China

⁷ Centro de Aplicaciones Tecnológicas y Desarrollo Nuclear (CEADEN), Havana, Cuba

⁸ Centro de Investigación y de Estudios Avanzados (CINVESTAV), Mexico City and Mérida, Mexico

⁹ Chicago State University, Chicago, Illinois, United States

¹⁰ China Institute of Atomic Energy, Beijing, China

¹¹ China University of Geosciences, Wuhan, China

¹² Chungbuk National University, Cheongju, Republic of Korea

¹³ Comenius University Bratislava, Faculty of Mathematics, Physics and Informatics, Bratislava, Slovak Republic

¹⁴ Creighton University, Omaha, Nebraska, United States

¹⁵ Department of Physics, Aligarh Muslim University, Aligarh, India

¹⁶ Department of Physics, Pusan National University, Pusan, Republic of Korea

¹⁷ Department of Physics, Sejong University, Seoul, Republic of Korea

¹⁸ Department of Physics, University of California, Berkeley, California, United States

¹⁹ Department of Physics, University of Oslo, Oslo, Norway

²⁰ Department of Physics and Technology, University of Bergen, Bergen, Norway

²¹ Dipartimento di Fisica, Università di Pavia, Pavia, Italy

²² Dipartimento di Fisica dell'Università and Sezione INFN, Cagliari, Italy

²³ Dipartimento di Fisica dell'Università and Sezione INFN, Trieste, Italy

²⁴ Dipartimento di Fisica dell'Università and Sezione INFN, Turin, Italy

²⁵ Dipartimento di Fisica e Astronomia dell'Università and Sezione INFN, Bologna, Italy

²⁶ Dipartimento di Fisica e Astronomia dell'Università and Sezione INFN, Catania, Italy

²⁷ Dipartimento di Fisica e Astronomia dell'Università and Sezione INFN, Padova, Italy

²⁸ Dipartimento di Fisica 'E.R. Caianiello' dell'Università and Gruppo Collegato INFN, Salerno, Italy

²⁹ Dipartimento DISAT del Politecnico and Sezione INFN, Turin, Italy

³⁰ Dipartimento di Scienze MIFT, Università di Messina, Messina, Italy

³¹ Dipartimento Interateneo di Fisica 'M. Merlin' and Sezione INFN, Bari, Italy

- ³² European Organization for Nuclear Research (CERN), Geneva, Switzerland
- ³³ Faculty of Electrical Engineering, Mechanical Engineering and Naval Architecture, University of Split, Split, Croatia
- ³⁴ Faculty of Engineering and Science, Western Norway University of Applied Sciences, Bergen, Norway
- ³⁵ Faculty of Nuclear Sciences and Physical Engineering, Czech Technical University in Prague, Prague, Czech Republic
- ³⁶ Faculty of Physics, Sofia University, Sofia, Bulgaria
- ³⁷ Faculty of Science, P.J. Šafárik University, Košice, Slovak Republic
- ³⁸ Frankfurt Institute for Advanced Studies, Johann Wolfgang Goethe-Universität Frankfurt, Frankfurt, Germany
- ³⁹ Fudan University, Shanghai, China
- ⁴⁰ Gangneung-Wonju National University, Gangneung, Republic of Korea
- ⁴¹ Gauhati University, Department of Physics, Guwahati, India
- ⁴² Helmholtz-Institut für Strahlen- und Kernphysik, Rheinische Friedrich-Wilhelms-Universität Bonn, Bonn, Germany
- ⁴³ Helsinki Institute of Physics (HIP), Helsinki, Finland
- ⁴⁴ High Energy Physics Group, Universidad Autónoma de Puebla, Puebla, Mexico
- ⁴⁵ Horia Hulubei National Institute of Physics and Nuclear Engineering, Bucharest, Romania
- ⁴⁶ HUN-REN Wigner Research Centre for Physics, Budapest, Hungary
- ⁴⁷ Indian Institute of Technology Bombay (IIT), Mumbai, India
- ⁴⁸ Indian Institute of Technology Indore, Indore, India
- ⁴⁹ INFN, Laboratori Nazionali di Frascati, Frascati, Italy
- ⁵⁰ INFN, Sezione di Bari, Bari, Italy
- ⁵¹ INFN, Sezione di Bologna, Bologna, Italy
- ⁵² INFN, Sezione di Cagliari, Cagliari, Italy
- ⁵³ INFN, Sezione di Catania, Catania, Italy
- ⁵⁴ INFN, Sezione di Padova, Padova, Italy
- ⁵⁵ INFN, Sezione di Pavia, Pavia, Italy
- ⁵⁶ INFN, Sezione di Torino, Turin, Italy
- ⁵⁷ INFN, Sezione di Trieste, Trieste, Italy
- ⁵⁸ Inha University, Incheon, Republic of Korea
- ⁵⁹ Institute for Gravitational and Subatomic Physics (GRASP), Utrecht University/Nikhef, Utrecht, Netherlands
- ⁶⁰ Institute of Experimental Physics, Slovak Academy of Sciences, Košice, Slovak Republic
- ⁶¹ Institute of Physics, Homi Bhabha National Institute, Bhubaneswar, India
- ⁶² Institute of Physics of the Czech Academy of Sciences, Prague, Czech Republic
- ⁶³ Institute of Space Science (ISS), Bucharest, Romania
- ⁶⁴ Institut für Kernphysik, Johann Wolfgang Goethe-Universität Frankfurt, Frankfurt, Germany
- ⁶⁵ Instituto de Ciencias Nucleares, Universidad Nacional Autónoma de México, Mexico City, Mexico
- ⁶⁶ Instituto de Física, Universidade Federal do Rio Grande do Sul (UFRGS), Porto Alegre, Brazil
- ⁶⁷ Instituto de Física, Universidad Nacional Autónoma de México, Mexico City, Mexico
- ⁶⁸ iThemba LABS, National Research Foundation, Somerset West, South Africa
- ⁶⁹ Jeonbuk National University, Jeonju, Republic of Korea
- ⁷⁰ Johann-Wolfgang-Goethe Universität Frankfurt Institut für Informatik, Fachbereich Informatik und Mathematik, Frankfurt, Germany
- ⁷¹ Korea Institute of Science and Technology Information, Daejeon, Republic of Korea
- ⁷² KTO Karatay University, Konya, Turkey
- ⁷³ Laboratoire de Physique Subatomique et de Cosmologie, Université Grenoble-Alpes, CNRS-IN2P3, Grenoble, France
- ⁷⁴ Lawrence Berkeley National Laboratory, Berkeley, California, United States
- ⁷⁵ Lund University Department of Physics, Division of Particle Physics, Lund, Sweden
- ⁷⁶ Nagasaki Institute of Applied Science, Nagasaki, Japan
- ⁷⁷ Nara Women's University (NWU), Nara, Japan
- ⁷⁸ National and Kapodistrian University of Athens, School of Science, Department of Physics, Athens, Greece
- ⁷⁹ National Centre for Nuclear Research, Warsaw, Poland
- ⁸⁰ National Institute of Science Education and Research, Homi Bhabha National Institute, Jatni, India
- ⁸¹ National Nuclear Research Center, Baku, Azerbaijan
- ⁸² National Research and Innovation Agency - BRIN, Jakarta, Indonesia

- 83 Niels Bohr Institute, University of Copenhagen, Copenhagen, Denmark
- 84 Nikhef, National institute for subatomic physics, Amsterdam, Netherlands
- 85 Nuclear Physics Group, STFC Daresbury Laboratory, Daresbury, United Kingdom
- 86 Nuclear Physics Institute of the Czech Academy of Sciences, Husinec-Řež, Czech Republic
- 87 Oak Ridge National Laboratory, Oak Ridge, Tennessee, United States
- 88 Ohio State University, Columbus, Ohio, United States
- 89 Physics department, Faculty of science, University of Zagreb, Zagreb, Croatia
- 90 Physics Department, Panjab University, Chandigarh, India
- 91 Physics Department, University of Jammu, Jammu, India
- 92 Physics Program and International Institute for Sustainability with Knotted Chiral Meta Matter (SKCM2), Hiroshima University, Hiroshima, Japan
- 93 Physikalisches Institut, Eberhard-Karls-Universität Tübingen, Tübingen, Germany
- 94 Physikalisches Institut, Ruprecht-Karls-Universität Heidelberg, Heidelberg, Germany
- 95 Physik Department, Technische Universität München, Munich, Germany
- 96 Politecnico di Bari and Sezione INFN, Bari, Italy
- 97 Research Division and ExtreMe Matter Institute EMMI, GSI Helmholtzzentrum für Schwerionenforschung GmbH, Darmstadt, Germany
- 98 Saga University, Saga, Japan
- 99 Saha Institute of Nuclear Physics, Homi Bhabha National Institute, Kolkata, India
- 100 School of Physics and Astronomy, University of Birmingham, Birmingham, United Kingdom
- 101 Sección Física, Departamento de Ciencias, Pontificia Universidad Católica del Perú, Lima, Peru
- 102 Stefan Meyer Institut für Subatomare Physik (SMI), Vienna, Austria
- 103 SUBATECH, IMT Atlantique, Nantes Université, CNRS-IN2P3, Nantes, France
- 104 Sungkyunkwan University, Suwon City, Republic of Korea
- 105 Suranaree University of Technology, Nakhon Ratchasima, Thailand
- 106 Technical University of Košice, Košice, Slovak Republic
- 107 The Henryk Niewodniczanski Institute of Nuclear Physics, Polish Academy of Sciences, Cracow, Poland
- 108 The University of Texas at Austin, Austin, Texas, United States
- 109 Universidad Autónoma de Sinaloa, Culiacán, Mexico
- 110 Universidade de São Paulo (USP), São Paulo, Brazil
- 111 Universidade Estadual de Campinas (UNICAMP), Campinas, Brazil
- 112 Universidade Federal do ABC, Santo Andre, Brazil
- 113 Universitatea Nationala de Stiinta si Tehnologie Politehnica Bucuresti, Bucharest, Romania
- 114 University of Cape Town, Cape Town, South Africa
- 115 University of Derby, Derby, United Kingdom
- 116 University of Houston, Houston, Texas, United States
- 117 University of Jyväskylä, Jyväskylä, Finland
- 118 University of Kansas, Lawrence, Kansas, United States
- 119 University of Liverpool, Liverpool, United Kingdom
- 120 University of Science and Technology of China, Hefei, China
- 121 University of South-Eastern Norway, Kongsberg, Norway
- 122 University of Tennessee, Knoxville, Tennessee, United States
- 123 University of the Witwatersrand, Johannesburg, South Africa
- 124 University of Tokyo, Tokyo, Japan
- 125 University of Tsukuba, Tsukuba, Japan
- 126 Universität Münster, Institut für Kernphysik, Münster, Germany
- 127 Université Clermont Auvergne, CNRS/IN2P3, LPC, Clermont-Ferrand, France
- 128 Université de Lyon, CNRS/IN2P3, Institut de Physique des 2 Infinis de Lyon, Lyon, France
- 129 Université de Strasbourg, CNRS, IPHC UMR 7178, F-67000 Strasbourg, France, Strasbourg, France
- 130 Université Paris-Saclay, Centre d'Etudes de Saclay (CEA), IRFU, Département de Physique Nucléaire (DPhN), Saclay, France
- 131 Université Paris-Saclay, CNRS/IN2P3, IJCLab, Orsay, France
- 132 Università degli Studi di Foggia, Foggia, Italy
- 133 Università del Piemonte Orientale, Vercelli, Italy
- 134 Università di Brescia, Brescia, Italy
- 135 Variable Energy Cyclotron Centre, Homi Bhabha National Institute, Kolkata, India

¹³⁶ Warsaw University of Technology, Warsaw, Poland

¹³⁷ Wayne State University, Detroit, Michigan, United States

¹³⁸ Yale University, New Haven, Connecticut, United States

¹³⁹ Yonsei University, Seoul, Republic of Korea

¹⁴⁰ Affiliated with an institute covered by a cooperation agreement with CERN

¹⁴¹ Affiliated with an international laboratory covered by a cooperation agreement with CERN.